

*Particle-in-cell experiments examine electron diffusion by whistler-mode waves: 1. Benchmarking with a cold plasma*

Article

Accepted Version

Allanson, O., Watt, C., Ratcliffe, H., Meredith, N., Allison, H., Bentley, S., Bloch, T. and Glauert, S. (2019) Particle-in-cell experiments examine electron diffusion by whistler-mode waves: 1. Benchmarking with a cold plasma. *Journal of Geophysical Research - Space Physics*, 124 (11). pp. 8893-8912. ISSN 0148-0227 doi:  
<https://doi.org/10.1029/2019JA027088> Available at  
<https://centaur.reading.ac.uk/86158/>

It is advisable to refer to the publisher's version if you intend to cite from the work. See [Guidance on citing](#).

To link to this article DOI: <http://dx.doi.org/10.1029/2019JA027088>

Publisher: American Geophysical Union

All outputs in CentAUR are protected by Intellectual Property Rights law, including copyright law. Copyright and IPR is retained by the creators or other copyright holders. Terms and conditions for use of this material are defined in the [End User Agreement](#).

[www.reading.ac.uk/centaur](http://www.reading.ac.uk/centaur)

**CentAUR**

Central Archive at the University of Reading

Reading's research outputs online

1           **Particle-in-cell experiments examine electron diffusion by**  
2           **whistler-mode waves: 1. Benchmarking with a cold plasma**

3           **O. Allanson<sup>1</sup>, C. E. J. Watt<sup>1</sup>, H. Ratcliffe<sup>2</sup>, N. P. Meredith<sup>3</sup>, H. J. Allison<sup>3,4</sup>, S. N. Bentley<sup>1</sup>, T.**  
4           **Bloch<sup>1</sup> & S. A. Glauert<sup>3</sup>**

5           <sup>1</sup>Space & Atmospheric Electricity Group; Department of Meteorology; University of Reading; Reading; UK

6           <sup>2</sup>Centre for Fusion, Space and Astrophysics; Department of Physics; University of Warwick; Coventry; UK

7           <sup>3</sup>British Antarctic Survey, Natural Environment Research Council, Cambridge; UK

8           <sup>4</sup>Helmholtz Centre Potsdam - GFZ German Research Centre for Geosciences; Potsdam; Germany

9           **Key Points:**

- 10           • Particle-in-cell numerical experiments track electron pitch-angle diffusion due to  
11           whistler-mode wave-particle interactions
- 12           • Our novel approach directly extracts diffusive characteristics across all energy and  
13           pitch angle space
- 14           • After an initial transient phase we observe a normal diffusive response that is con-  
15           sistent with quasilinear theory

---

Corresponding author: Oliver Allanson, o.allanson@reading.ac.uk

## Abstract

Using a particle-in-cell code, we study the diffusive response of electrons due to wave-particle interactions with whistler-mode waves. The relatively simple configuration of field-aligned waves in a cold plasma is used in order to benchmark our novel method, and to compare with previous works that used a different modelling technique. In this boundary-value problem, incoherent whistler-mode waves are excited at the domain boundary, and then propagate through the ambient plasma. Electron diffusion characteristics are directly extracted from particle data across all available energy and pitch-angle space. The ‘nature’ of the diffusive response is itself a function of energy and pitch-angle, such that the rate of diffusion is not always constant in time. However, after an initial transient phase, the rate of diffusion tends to a constant, in a manner that is consistent with the assumptions of quasilinear diffusion theory. This work establishes a framework for future investigations on the nature of diffusion due to whistler-mode wave-particle interactions, using particle-in-cell numerical codes with driven waves as boundary value problems.

## Plain language summary

‘Whistler-mode’ plasma waves interact with electrons in the Earth’s outer radiation belts. This wave-particle interaction plays a significant role in both electron acceleration, and in the loss of electrons to the atmosphere via ‘pitch angle scattering’. Such processes are typically modelled using numerical diffusion codes, with electron diffusion coefficients that characterize the nature and the strength of the wave-particle interaction. These diffusion coefficients are calculated using a mixture of long-established theory and input parameters taken from data and/or empirical models. We present a novel method for the direct extraction of characteristics of the electron diffusion from particle-in-cell numerical experiments. Our results demonstrate that the rate of diffusion can be time-dependent at early times, but then tends to constant values in a manner that is consistent with quasilinear theory.

## 1 Introduction

Wave-particle interactions are a key source of variability in the outer radiation belt (e.g. *Horne et al.* [2005a]; *Thorne* [2010]; *Reeves et al.* [2013]). Decades of research into the behaviour of high-energy electrons in Earth’s magnetosphere has determined that wave-particle interactions over a range of different frequencies can diffuse the particles in phase-space, leading to energisation and loss of high-energy particles that could explain the variability of the belts (e.g. *Fälthammar* [1965]; *Hudson et al.* [2000]; *Thorne et al.* [2013]). Whistler-mode waves are electromagnetic waves that propagate below the electron gyrofrequency (e.g. see *Artemyev et al.* [2016a]) and can interact with electrons across a wide range of energies (e.g. *Horne et al.* [2005b]; *Thorne et al.* [2010]). Whistler-mode waves take a range of different forms: narrowband transmitter waves are artificially-generated at Earth’s surface by high-power radio transmitters (e.g. *Zhang et al.* [2018b]; *Meredith et al.* [2019]); lightning-generated whistlers are generated by lightning and propagate upwards through the ionosphere into the magnetosphere (e.g. *Němec et al.* [2010]); whistler-mode chorus is naturally generated by plasma instabilities within the Earth’s magnetosphere (e.g. *Omura et al.* [2007]; *Meredith et al.* [2009]; *Chen et al.* [2017]; *Gao et al.* [2017]); incoherent plasmaspheric hiss [*Bortnik et al.*, 2008a; *Chen et al.*, 2012, 2014] has a number of established source mechanisms (e.g. see *Meredith et al.* [2018] for a discussion of these).

Current approaches to modelling the effect of wave-particle interactions in the outer radiation belt most typically use the quasilinear theory (QLT) [*Kennel and Engelmann*, 1966; *Lerche*, 1968; *Lyons*, 1974]. This formalism describes wave-particle interactions as diffusive processes in the plasma, flattening out gradients and moving electrons to different energies and/or different pitch-angles. The exact form of the equations used in the model depends on the characterization of the wave-particle interactions that are responsible for

66 the diffusive behaviour, and this characterization is provided by the diffusion coefficients.  
 67 The analytic form of diffusion coefficients are derived using QLT, and then implemented  
 68 in diffusion codes by using models of wave and plasma parameters (e.g. see *Glauert et al.*  
 69 [2014]). Formally, the application of QLT to wave-particle interactions places a number  
 70 of restrictions on the plasma waves considered, typically considered to be that the waves  
 71 are incoherent and of low amplitude [*Stix*, 1992; *Treumann and Baumjohann*, 2001]. How-  
 72 ever, observations of whistler-mode waves in the inner magnetosphere (e.g. *Cattell et al.*  
 73 [2008]; *Cully et al.* [2008]; *Breneman et al.* [2011]; *Wilson III et al.* [2011]; *Kellogg et al.*  
 74 [2011]; *Gao et al.* [2016]) have revealed that wave amplitudes can be orders of magnitude  
 75 larger than previously thought. Furthermore, it is evident from observations that certain  
 76 whistler-modes possess structure and/or coherency in frequency space, e.g. the rising and  
 77 falling tones of chorus emissions, and the nearly monochromatic signals of transmitter  
 78 waves. Hence there is strong evidence that motivates from-first-principles investigations of  
 79 whistler-mode wave-particle interactions in the outer radiation belt.

80 There are a large number of theoretical calculations and numerical experiments rele-  
 81 vant to the work presented in this paper and so it is not possible to discuss every one (e.g.  
 82 a non-exhaustive list of such works on whistler-mode wave-particle interactions includes  
 83 *Albert* [2001, 2002]; *Omura et al.* [2007]; *Bortnik et al.* [2008b]; *Albert* [2010]; *Tao and*  
 84 *Bortnik* [2010]; *Tao et al.* [2011, 2012a,b, 2013]; *Camporeale and Zimbardo* [2015]; *Cam-*  
 85 *poreale* [2015]; *Mourenas et al.* [2018]; *Silva et al.* [2018]). Instead, we focus on some of  
 86 the works that - either with test-particle or particle-in-cell (PiC) codes - analyzed the sta-  
 87 tistical/diffusive response of the plasma, by directly extracting particle data. *Bortnik et al.*  
 88 [2008a] used test-particle experiments in a dipolar magnetic field to model the effect of  
 89 large amplitude and oblique monochromatic chorus waves on the particle response. It was  
 90 found that the wave-particle interaction changed qualitatively from that of diffusion be-  
 91 yond a certain amplitude, in which case a nonlinear approach was found necessary. The  
 92 nature of the nonlinear behaviour observed (diffusive, phase bunching or phase-trapping)  
 93 was found to correlate with those predicted in *Albert* [2002] for different wave and plasma  
 94 regimes. The nonlinear behaviour also varies according to a inhomogeneity parameter  
 95 that indicates whether or not quasi-linear theory is applicable in the narrowband limit  
 96 (discussed in e.g. *Bortnik et al.* [2008a]; *Omura et al.*; *Tao and Bortnik* [2010]; *Tao et al.*  
 97 [2012a]). *Tao et al.* [2011] used a test-particle code to study the response of electrons to a  
 98 uniform spectrum of incoherent, broadband and small amplitude waves in a homogeneous  
 99 background field, but specifically targeted electron populations predicted to be in reso-  
 100 nance. They found that the electron response was indeed stochastic and in excellent agree-  
 101 ment with QLT. *Tao et al.* [2012a] performed test-particle simulations for field-aligned  
 102 waves in a simplified dipole field model (no curvature), and found (also for resonant par-  
 103 ticles only) that the bounce-averaged quasi-linear diffusion coefficients became invalid as  
 104 the wave amplitude surpassed given thresholds. Specifically, they found this threshold to  
 105 be  $|B_{w,rms}^2/B_0^2| \geq 2 \times 10^{-7}$  for 10keV electrons, and  $|B_{w,rms}^2/B_0^2| \geq 7 \times 10^{-6}$  for 1MeV  
 106 electrons, where waves have root-mean-squared amplitudes of magnitude  $B_{w,rms}$  in a back-  
 107 ground field  $B_0$ . *Camporeale and Zimbardo* [2015] used self-consistent kinetic simulations  
 108 to investigate diffusion during the linear growth phase and saturation of anisotropy-driven  
 109 instabilities that self-consistently generate whistler-mode waves. They found evidence of  
 110 nonlinear and time-dependent effects, with enhanced pitch angle diffusion during the linear  
 111 growth phase. In a similar experiment, *Camporeale* [2015] investigated diffusion due to  
 112 the self-consistently generated lower-band chorus waves, and compared to the predictions  
 113 given by a QLT diffusion code. Specifically, they found significant mismatch in regions  
 114 of phase-space for which the resonance condition is not satisfied, and called for nonlin-  
 115 ear theories in order to capture non-resonant interactions. We also note that there is re-  
 116 cent theoretical work based upon using kinetic equations used to describe the evolution of  
 117 the particle energy distribution due to nonlinear wave-particle interactions *Artemyev et al.*  
 118 [2016b, 2017, 2018]; *Mourenas et al.* [2018]; *Vainchtein et al.* [2018], and for which one  
 119 of the main aims is “to incorporate nonlinear effects of intense, short-duration chorus wave  
 120 packets into global (quasilinear) diffusion models” (Quoted from presentation, J. Bortnik,

ISSS-13, September 6-14 2018, UCLA). We note that the standard quasilinear diffusion theory sometimes captures observed diffusive properties surprisingly well, even in circumstances for which the assumptions of the theory are formally invalid (e.g. see a discussion in *Zhang et al.* [2018a]).

The standard test-particle approach to modelling wave-particle interactions presents both advantages and disadvantages. Test-particle codes are (relatively) cheap to run numerically and enable one to implement wave modes of exactly the desired form. However, wave-particle interactions are a fundamentally kinetic physics process, and test-particle codes do not include all of the self-consistent interactions between particles and wave fields. Particle-in-cell experiments enable users to model these self-consistent interactions, and in principle allow a greater range of kinetic-physics diagnostics (e.g. the distribution function). Indeed, it has recently been shown that using the two different approaches to study diffusion due to whistler mode wave-particle interactions can yield markedly different results [*Camporeale and Zimbardo, 2015; Camporeale, 2015*]. Here, we use a mixture of both the test-particle and particle-in-cell approaches. We exploit the self-consistent PiC interaction to model the waves as they propagate through the plasma, instead of prescribing fixed-characteristic waves as in a test-particle approach. The inclusion of sub electron-scale physics in the interaction between the background plasma and the propagating waves will allow the whistler-mode waves to fluctuate on sub-electron spatial and temporal scales. In the simulation, we release a very large number of tracer ('test') particles in order to extract characteristics of the pitch-angle diffusion for electrons across all available energies and pitch-angles. These tracer particles contribute no 'moments' to the particle-in-cell algorithm, and respond to the electromagnetic fields in the same way as the methods in *Tao et al.* [2011], for example. In using a combination of both self-consistent particle-in-cell and test-particle methods, we should expect to see both similarities and differences in the results obtained when compared to *Tao et al.* [2011].

In particular, our intent in this first paper of a series is to study the nature of the diffusion when the waves propagate in one dimension along the background magnetic field in a cold, homogeneous plasma. This initial 'benchmarking' scenario showcases our method and indicates similarities to and differences from the test-particle results reported in previous work (e.g. *Tao et al.* [2011]). Future papers in this series will compare the strength of the effective diffusion coefficients extracted from the PiC experiment with the size of the analytic quasilinear diffusion coefficient across all of pitch-angle/energy space, and will repeat the numerical experiment for whistler-mode wave propagation through a plasma with the fractional warm components that can be found in Earth's inner magnetosphere.

This paper is organized as follows. In Section 2 we describe the philosophy and setup of the numerical experiments, including the numerical scheme. In particular we discuss the wave excitation mechanism and the properties of the electromagnetic waves within the domain. Diffusion theory as is applicable to the outer radiation belt is discussed in Section 3. Results from the numerical experiments, including the diffusive plasma response are discussed in Section 4. In Section 5 we discuss our results in more detail and put the results in context. Section 6 contains a summary, including motivation for future investigations that will build upon the results reported here.

## 2 Outline of experiments

Radiation belt diffusion coefficients are fundamentally a function of both the plasma and wave parameters, i.e., the plasma density, background magnetic field, wave strength and wave spectral form. As a result, the direct evaluation of a diffusion coefficient relies on both the plasma and wave characteristics being quasi-static for the time over which they are calculated [*Schulz and Lanzerotti, 1974*]. Therefore we consider a boundary value problem, in which we perturb the left-hand boundary with a given specific wave spectrum, which then excites electromagnetic waves that propagate throughout the experimental do-

172 main. The perturbation mechanism is applied at all times, and this enables us to study  
 173 the interaction for a wave spectrum that is quasi-static in amplitude (root-mean-squared)  
 174 and spectral form. However, the wave spectrum does exhibit some small-scale spatial and  
 175 temporal fluctuations in response to self-consistent interactions with the background cold  
 176 plasma. This approach is in contrast to an initial value problem, in which one might study  
 177 the self-consistent generation mechanism and subsequent evolution of waves in an initially  
 178 unstable plasma, and for which the wave spectra is more variable in time (e.g. *Katoh and*  
 179 *Omura* [2006]; *Omura et al.*; *Hikishima et al.* [2009]; *Omura et al.* [2009]; *Omidi et al.*  
 180 [2010, 2011]; *Katoh and Omura* [2013]; *Camporeale* [2015]; *Camporeale and Zimbardo*  
 181 [2015]; *Silva et al.* [2017]; *Ratcliffe and Watt* [2017]; *Katoh et al.* [2018]). In *Tao et al.*  
 182 [2011], a relativistic test-particle code was used to study the diffusive plasma response  
 183 due to wave-particle interactions of driven, broadband and incoherent waves waves with  
 184 magnetospheric plasma populations appropriate for the outer radiation belt at 6 Earth radii  
 185 ( $r \sim 6R_E$ ). Our experimental parameters are chosen in order to resemble those in *Tao et al.*  
 186 [2011] as far as possible.

## 187 2.1 Numerical experiment design

188 Wave-particle interactions are a fundamentally kinetic plasma physics process, since  
 189 their efficiency explicitly depends on particle-scale physics, as statistically described by the  
 190 particle distribution function. We use the EPOCH PiC code [*Arber et al.*, 2015], which is  
 191 described in more detail in Appendix A. Essentially, the numerical experiments involve  
 192 exciting waves of specified frequencies from an "antenna" at one of the spatial boundaries  
 193 of the simulation domain. Electromagnetic waves then propagate through the domain, self-  
 194 consistently interacting with the cold plasma component of the plasma interior. We also  
 195 release a large number of non-interacting 'tracer' particles that are used to monitor the  
 196 diffusion in different regions of pitch-angle/energy space. These particles contribute no  
 197 moments to the PiC algorithm. The tracer particles act as 'labels' in phase-space such  
 198 that their collective diffusive response can be categorized as a function of pitch angle and  
 199 energy.

200 As a first step, we restrict the experimental domain to one field-aligned dimension  
 201 ( $x$ ). On the compressed dayside magnetosphere near the magnetic equator, uniform fields  
 202 and field-aligned wave propagation is a reasonable approximation [*Tsurutani and Smith,*  
 203 1977]. We do so in order to fully understand the most idealized example of this wave-  
 204 particle interaction, before introducing new effects in isolation (e.g. oblique wave propaga-  
 205 tion, field inhomogeneities, and modifications to the wave spectra). EPOCH uses a Carte-  
 206 sian grid, which in 1-D means that all quantities may vary in the  $x$  direction only. We set  
 207 an ambient magnetic field,  $\mathbf{B}_0 = (B_{x0}, 0, 0)$ , with  $B_{x0} = 140\text{nT}$ , and so refer to  $x$  as parallel  
 208 ( $\parallel$ ),  $y$  and  $z$  as perpendicular ( $\perp$ ).

209 We model a uniform cold 'background' plasma with number density,  $n_b = 10^7\text{m}^{-3}$ .  
 210 For this cold background plasma, and ambient magnetic field, the ratio of electron plasma  
 211 frequency to non-relativistic gyrofrequency is given by  $\omega_{pe}/|\omega_{ce}| \approx 7.2$ , for  $\omega_{pe} = \sqrt{ne^2/(m_e\epsilon_0)}$ ,  
 212 and  $\omega_{ce} = q_e B_0/m_e < 0$  in the uniform background field. We describe the ambient  
 213 plasma by using cold ion and electron populations with initial spatially uniform number  
 214 density of  $n_b$  and isotropic temperature of 0.1eV. These choices are motivated by our de-  
 215 sire to emulate, as far as possible, the scenario of *Tao et al.* [2011]. In a warm plasma, or  
 216 plasma with fractional warm components, the wave amplitudes would be expected to al-  
 217 tered by the presence of the warm component. If the plasma is isotropic, then the waves  
 218 will damp/reduce their amplitude, and if the plasma has positive anisotropy then the waves  
 219 may grow in amplitude through the appropriate kinetic wave-particle interaction. In this  
 220 numerical experiment, we choose a cold plasma environment in order to ensure that waves  
 221 entering the domain do not change amplitude significantly as they propagate through the  
 222 plasma.

The real world run time for the experiment is  $T = 575t_{ce} \approx 0.15\text{s}$ , for  $t_{ce} = 1/f_{ce}$  with  $f_{ce} = |\omega_{ce}|/(2\pi) \approx 3919\text{Hz}$ . We use 500 particles-per-cell per species; physical values of proton-electron mass ratio,  $m_i/m_e = 1836.2$ ; and the speed of light is set to its real value  $c \approx 3 \times 10^8\text{ms}^{-1}$ . Periodic boundary conditions are chosen for the particles, whereas electromagnetic waves have open boundary conditions (the electromagnetic field boundary condition works by allowing outflowing characteristics to propagate through the boundary with as little reflection as possible). The domain length,  $L = 40\lambda_{ic}$ , is set to be 40 times the estimated wavelength inside the domain,  $\lambda_{ic} = c/(\eta f_{ic})$ , of the lowest frequency wave emitted by the antenna,  $\omega_{ic} = 2\pi f_{ic}$ . The refractive index is a function of frequency,  $\eta = \eta(\omega)$ , and is determined by the cold plasma dispersion relation [Stix, 1992; Omura *et al.*, 2007],

$$\eta^2 = \frac{c^2 k^2}{\omega^2} = 1 + \frac{\omega_{pe}^2/\omega^2}{|\omega_{ce}|/\omega - 1}. \quad (1)$$

We use 3587 cells in the  $x$ -direction, with grid spacing  $\Delta x \approx 235\text{m}$ , such that  $\Delta x/(c/|\omega_{ce}|) \approx 0.02$ . The Debye radius,  $\lambda_D = \sqrt{\epsilon_0 k_B T_e / (n_b q_e^2)} \approx 2.35\text{m}$  is not resolved by  $\Delta x$ , and we have  $\Delta x/\lambda_D = 100$ . It is well-known that particle-in-cell experiments are in principle vulnerable to the self-heating phenomenon, and that this can be mitigated by choosing  $\Delta x \approx \lambda_D$  in explicit codes. However, it is absolutely possible to perform valid and physically meaningful particle-in-cell numerical experiments with a value of  $\Delta x$  that does not resolve the Debye radius (e.g. see a discussion in [Arber *et al.*, 2015]). In particular, if one can demonstrate that for a particular choice of  $\Delta x$ :

1. all necessary physical scales have been resolved that are most important for the phenomenon of interest,
2. the self-heating is limited to a reasonable level,

then it is entirely justifiable to have  $\Delta x > \lambda_D$ . It is not uncommon to use such values, e.g. two examples of works that discussed results of explicit PiC experiments using a spatial resolution  $\Delta \gg \lambda_D$  include: (i) *Ratcliffe and Watt* [2017] with  $\Delta/\lambda_D \approx 139$ , in which the ‘0.5 cyclotron frequency gap’ in magnetospheric whistler-mode waves was self-consistently generated; (ii) *Tsiklauri* [2016] with  $\Delta/\lambda_D \approx 200 - 270$ , for the study of electron plasma wakefield acceleration.

We justify point 1. for our experiment as follows. Our chosen value of  $\Delta x$  resolves the electron inertial length according to  $\Delta x/d_e \approx 0.07$ , for  $d_e = c/\omega_{pe} \approx 1680\text{m}$ , and therefore resolves the fundamental scale of electron kinetic physics. Furthermore, it resolves the shortest wavelength of the whistler-mode wave spectrum that is important for the wave-particle dynamics in this study,  $\Delta x/\lambda_{uc} \approx 0.009$ , for  $\lambda_{uc} = c/(\eta f_{uc})$  and  $\eta$  determined by equation (1). Therefore, our chosen grid discretization resolves electron scale kinetic physics, and in particular the spatial scales necessary for electron wave-particle interactions with the driven whistler-mode waves.

We justify point 2. for our experiment as follows. The classic constraint  $\Delta x \approx \lambda_D$  [Langdon, 1970] relates to the case where particle forces are assigned to ‘nearest-neighbour’ grid points, and for which the underlying scheme is momentum-conserving. EPOCH is a charge-conserving code, with capability to use higher-order shape functions: such weighting schemes suffer from a less catastrophic form of self-heating, and generally with a low growth rate. In this work we triangular shape functions (a 3 point stencil, 2 cells wide). A discussion of stability and self-heating in EPOCH, with reference to shape-functions, is given in Section 5 of *Arber et al.* [2015]. The EPOCH code also provides one further method to limit the noise in the PiC simulation, and which we use in this work: ‘ $\delta F$  mode’ (as detailed in Appendix A). In figure 1 we present an analysis of the temporal evolution of the electromagnetic and particle energies within the experimental domain, with special consideration of the electromagnetic energy flux through the boundaries. The experiment utilizes periodic boundary conditions for the particles. However, there is a constant input of electromagnetic energy into the domain via the wave excitation method,



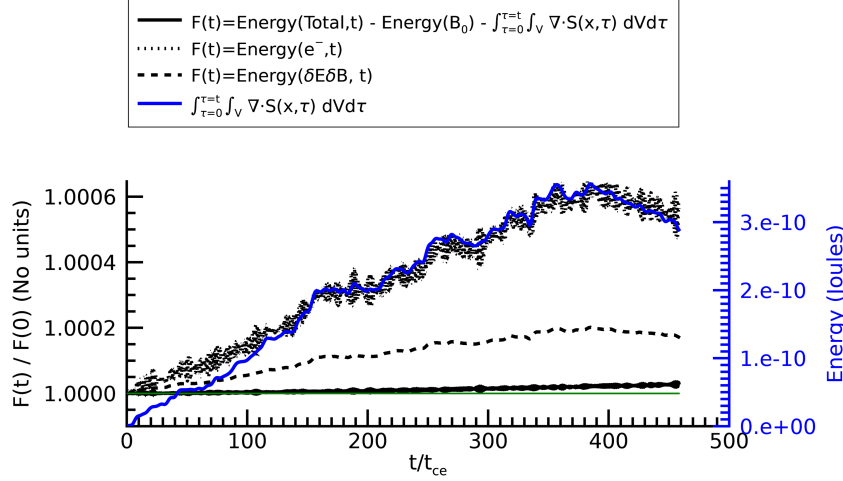


Figure 1. Evolution of the energy budget within the experiment.

and outgoing electromagnetic wave energy is permitted to flow out of the experimental domain. Therefore the total energy will not be conserved, but the following quantity should be conserved,

$$E_{KE}(t) + E_{EM, \text{domain}}(t) - E_{S, \text{boundary}}(t) = \text{const.} \quad (2)$$

The three terms on the left-hand-side represent, respectively: (a) the kinetic energy of all ions and electrons; (b) the total electromagnetic energy within the domain; (c) the time-integrated net electromagnetic power that has entered the domain up to time  $t$ ,

$$E_{S, \text{boundary}}(t) := \int_{\tau=0}^t \int_V \nabla \cdot \mathbf{S}(x, t) dV d\tau$$

for  $\mathbf{S}$  the Poynting vector. This time-integrated power (energy) represents the only means by which the total energy budget within the experimental domain should change. In figure 1 we plot the normalized evolution of the quantity in equation (2) minus the energy associated with the time-independent and homogeneous background magnetic field (with a solid black line). Stability of the numerical code required that this quantity should not diverge significantly from unity. Figure 1 shows conservation of the net simulation energy to better than 0.1%, confirming that self heating is minimal. In figure 1 we also plot the evolution of: total electron energy (black dots); total energy associated with electromagnetic fluctuations within the domain (black dashes); and the time-integrated electromagnetic power that has entered the domain up to time  $t$  (solid blue line). We see that the total electron energy clearly tracks the injected wave energy and the total energy associated with the EM fluctuations.

## 2.2 Wave spectra

We excite the plasma at the left-hand boundary ( $x = 0$ ) using EPOCH's using EPOCH's driven boundary option, (called 'laser' after its most common use), such that the perturbations propagate in the positive- $x$  direction. For each given specified frequency, this boundary condition simply perturbs the domain with a (sinusoidal) time-varying electromagnetic field. We superpose a collection of different perturbations, with the intent to reproduce the spectrum used in *Tao et al.* [2011]. We specify a discrete sum of  $N_{\text{wave}} = 100$  individual right-hand polarized electric field perturbations. Each one of the 100 modes

300 is composed of 2 linearly polarized components, with wave fields that oscillate in the  $y$   
 301 and  $z$  directions respectively,

$$\mathbf{E}_{\text{wave}}(x, t) = \sum_{i=1}^{N_{\text{wave}}} \mathbf{E}_{\text{wave},i}(x, t) = \sum_{i=1}^{N_{\text{wave}}} \mathbf{E}_{\text{wave},y,i}(x, t) + \mathbf{E}_{\text{wave},z,i}(x, t),$$

302 Each pair of linearly polarized waves,  $(\mathbf{E}_{\text{wave},y,i}, \mathbf{E}_{\text{wave},z,i})$ , has the appropriate phase shift  
 303 between themselves such as is required for right-handed polarization [Stix, 1992]. Each  
 304 mode,  $\mathbf{E}_{\text{wave},i}$ , also has a random phase, and a frequency that is uniformly selected from  
 305 the range

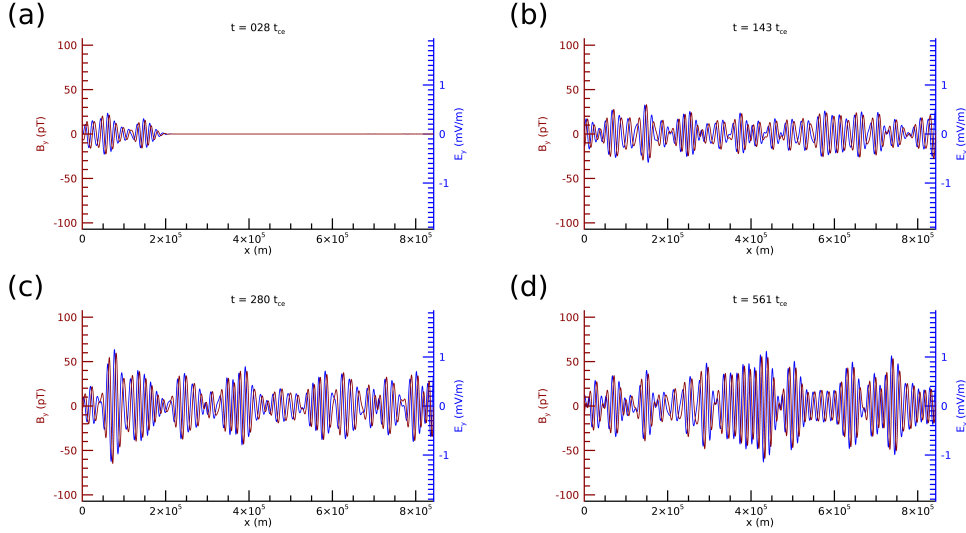
$$f_{lc} = 0.2f_{ce} \leq f \leq 0.4f_{ce} = f_{uc}.$$

306 Full details on how to prescribe such a spectrum are given in *Tao et al.* [2011], and we  
 307 include the text file that prescribes the perturbation as supplementary information (S2).

308 Given these user inputs for the electric field perturbations, the Maxwell solver in  
 309 EPOCH generates self-consistent magnetic field perturbations ( $\mathbf{B}_{\text{wave},i}$ ) in accordance with  
 310 Maxwell's equations. We choose the magnitude of the electric field perturbations so that  
 311 they are (in principle) consistent with corresponding magnetic field perturbations of 1pT  
 312 in a vacuum ( $|\mathbf{E}_{\text{wave},i}| = c|\mathbf{B}_{\text{wave},i}|$ , and such that  $|\mathbf{B}_{\text{wave},i}| = 1\text{pT}$ ). We note here that  
 313 our perturbation method is intended to excite the whistler-mode wave branch of the cold  
 314 plasma dispersion relation [Stix, 1992], since a cold plasma can support whistler-mode  
 315 wave propagation when excited at these frequencies. A 'fully self-consistent' wave driv-  
 316 ing technique would also necessitate the self-consistent perturbations of other oscillat-  
 317 ing macroscopic quantities, e.g. polarization currents. However, that approach is much  
 318 more complicated and beyond the scope of this work. Regardless of the specific excitation  
 319 technique, and as will be shown, we are able to excite the electromagnetic component of  
 320 whistler-mode waves within the interior of the plasma. Once excited, these components  
 321 then propagate and continue to be supported by (and interact self-consistently with) the  
 322 background cold-plasma.

323 Sudden electromagnetic perturbations can often cause undesired 'shock' effects in  
 324 a simulated plasma at the moment the perturbation is 'switched on'. In order to eliminate  
 325 any such effects, we apply a linear envelope to the wave profile, so that for  $t < 2/f_{lc}$ ,  
 326 the wave profile has amplitude scaled by  $1/t$ . This prevents any shock effects from oc-  
 327 ccurring. It takes approximately  $t_{\text{cross}} = 115t_{ce}$  for the wave profile to cross the experi-  
 328 mental domain, from left to right. All wave and particle analysis in this paper pertains to  
 329 times after this time,  $t > t_{\text{cross}}$ . Therefore we analyze only over times during which the  
 330 entire experimental domain is interacting with the propagating waves. Since the run time  
 331 of the experiment is  $T = 575t_{ce}$ , we analyze wave-particle interactions for a total time of  
 332  $T - t_{\text{cross}} = 460t_{ce}$ . This corresponds to  $\approx 92$  wave periods for waves with frequency  $f_{lc}$ ,  
 333 and  $\approx 184$  wave periods for waves with frequency  $f_{uc}$ . For completeness, we plot the  $B_y$   
 334 (red) and  $E_y$  (blue) components of the electromagnetic fields as a function of  $x$  in figure  
 335 2. This figure includes the waveform at: (a)  $28t_{ce}$ , soon after the completion of the linear  
 336 envelope scaling of the excitation; (b)  $143t_{ce}$ , soon after the wave has crossed the domain;  
 337 (c)  $280t_{ce}$ , roughly half-way through the numerical experiment; (d)  $561t_{ce}$ , close to the end  
 338 of the experiment.

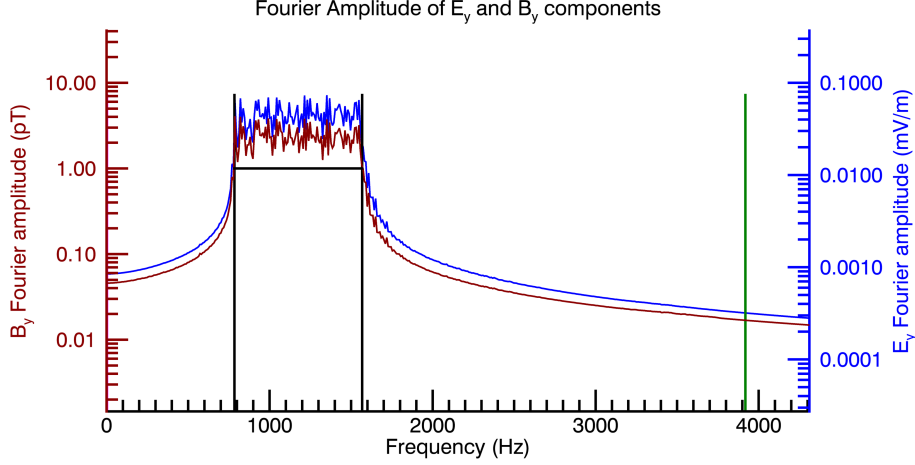
341 One important difference between our work and that of *Tao et al.* [2011], is that the  
 342 wave-spectrum excited by the antenna on the left-hand boundary is not exactly reproduced  
 343 within the domain. Since we use a fully kinetic numerical code, the driven waves interact  
 344 self-consistently with the background plasma populations via Maxwell's equations, where  
 345 the current density is derived directly from the flux of different species' super-particle  
 346 populations. The background plasma super-particle populations evolve in a self-consistent  
 347 manner via the (relativistic) Lorentz force equation. This is all at the cost of higher com-  
 348 putational expense, as compared to a test-particle simulation. However, we consider the  
 349 freedom to have fully self-consistent wave-particle interactions to be a benefit of using the



339 **Figure 2.** The  $B_y$  (red) and  $E_y$  (blue) components of the electromagnetic fields as a function of  $x$  at: (a)  
 340  $28t_{ce}$ ; (b)  $143t_{ce}$ ; (c)  $280t_{ce}$ ; (d)  $561t_{ce}$ .

350 PiC approach for this study, and therefore the benefits of using fully self-consistent PiC  
 351 compensate for the added computational cost.

359 Figure 3 shows the ‘one-sided’ Fourier amplitude spectrum of the  $B_y$  (red) and  $E_y$   
 360 components (blue) of the waves, averaged over all space (within the PiC domain) and  
 361 time during the wave-particle interaction ( $460t_{ce}$ , i.e.  $t > t_{cross}$ ). The Fourier amplitude  
 362 is defined such that a single wave  $\sim A \sin(kx \pm \omega t)$  will have amplitude  $|A|$ . The vertical  
 363 black lines mark the lower and upper bounds of the driven wave spectrum ( $f_{lc} = 0.2f_{ce}$   
 364 and  $f_{uc} = 0.4f_{ce}$  respectively), whilst the vertical green line marks the electron gyro-  
 365 frequency  $f_{ce}$ . The horizontal black line marks a continuous version of the  $B_y$  spectrum  
 366 employed by *Tao et al.* [2011]. The waves clearly show dominant power within the re-  
 367 quired frequency domain. However, there is some amplification as compared to the uni-  
 368 form 1pT spectrum as used by *Tao et al.* [2011], and we observe non-zero amplitudes  
 369 outside the driven frequency domain ( $f_{lc}, f_{uc}$ ). We observe a root-mean-square wave am-  
 370 plitude of  $B_{w,rms} \approx 25\text{pT}$  in our experiment, slightly higher than the value of 10pT that  
 371 *Tao et al.* [2011] use. This difference is, in reality, a small one, and a result of the diffi-  
 372 culty in exactly prescribing a given wave spectrum in a PiC experiment. This amplitude  
 373  $((B_{w,rms}/B_0)^2 \approx 3 \times 10^{-8})$  still falls well below the nonlinear wave amplitude thresholds  
 374 as discussed in Section 1. Therefore, this factor does not preclude us from comparing our  
 375 results to those obtained by *Tao et al.* [2011]. As discussed above, we excite the boundary  
 376 with individual whistler modes each with electric field amplitudes that correspond to mag-  
 377 netic field perturbations of 1pT, but for the case of a vacuum ( $|\delta\mathbf{B}| \approx |\delta\mathbf{E}|/c$ ). However,  
 378 when propagating through a plasma medium, one will expect magnetic field perturbations  
 379 within the domain  $|\delta\mathbf{B}| \approx |\delta\mathbf{E}|/(c/\eta)$  (in our experiment  $14.8 < \eta < 18.1$  for waves  
 380 with frequencies  $f_{lc} < f < f_{uc}$ ). If the coupling efficiency between the wave excitation  
 381 mechanism and the plasma was 100% efficient, then we should expect a spectrum of mag-  
 382 netic field perturbations (i.e. at each frequency) with amplitudes a factor of  $\eta$  greater than  
 383  $|\delta\mathbf{E}|/c$ , i.e.  $\approx \eta \times 1\text{pT}$ . However, the coupling is not perfectly efficient, as should be ex-  
 384 pected, and so we observe magnetic field perturbations within the domain  $\approx 2-3$  times the  
 385 1pT level used by *Tao et al.* [2011]. One obtains near-identical results as those in figure 3  
 386 for the power spectra of the  $B_z$  and  $E_z$  components, as should be expected for circularly  
 387 polarized waves.



352 **Figure 3.** Fourier amplitude of the  $B_y$  (red) and  $E_y$  components (blue) of the waves within the PiC do-  
 353 main. Vertical black lines mark the lower and upper bounds of the driven wave spectrum ( $f_{lc} = 0.2f_{ce}$  and  
 354  $f_{uc} = 0.4f_{ce}$  respectively). Vertical green line marks the electron gyrofrequency  $f_{ce}$ . The horizontal black  
 355 line marks a continuous version of the  $B_y$  spectrum employed by *Tao et al.* [2011].

388 Figure 4 shows the ‘dispersion relation’ of the  $B_y$  component of the waves present,  
 389 obtained via Fourier transforms performed over the entire spatial and temporal domain  
 390 during the wave-particle interaction. The over-plotted line marks the cold plasma disper-  
 391 sion relation as according to equation (1), and we see that the dominant power is strongly  
 392 localized to the  $(f_{lc}, f_{uc})$  region, and along the expected dispersion curve. Once again, we  
 393 obtain near-identical plots of the dispersion relation for  $B_z$ ,  $E_y$  and  $E_z$ .

### 394 3 Particle diffusion

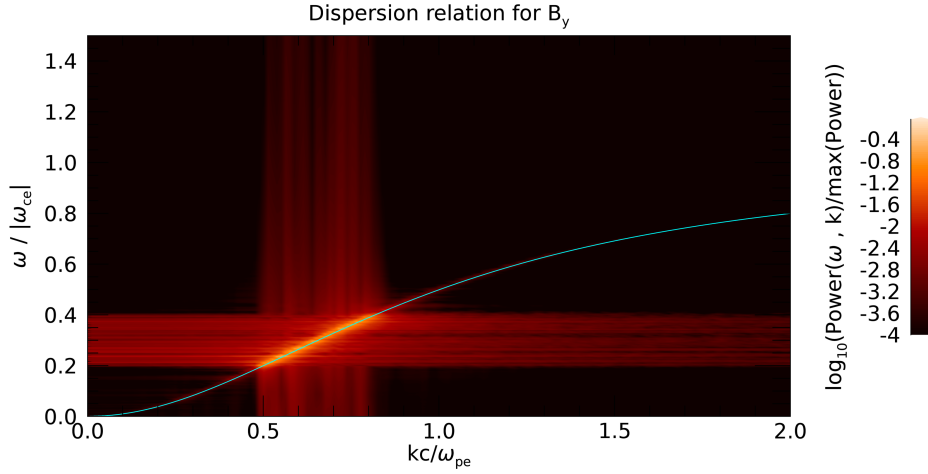
395 The application of QLT to the Vlasov-Maxwell equation for collisionless plasmas  
 396 leads to a diffusion equation to describe the plasma distribution function,  $F$ , of the form

$$\frac{\partial F}{\partial t} = \sum_{i,j} \frac{\partial}{\partial J_i} \left[ D_{ij} \frac{\partial F}{\partial J_j} \right] \quad (3)$$

397 [Schulz and Lanzerotti, 1974], for  $D_{ij}$  a symmetric tensor of diffusion coefficients, and  $J_i$   
 398 are the three action integrals associated with adiabatic charged particle motion [Northrop,  
 399 1963; Roederer and Zhang, 2013]. For use in the outer radiation belt, equation (3) is typ-  
 400 ically rewritten in  $(E, \alpha, L^*)$  space (e.g. see Glauert et al. [2014]). Here, the energy  $E =$   
 401  $p^2/(2m_{0e})$  (for  $\mathbf{p} = \gamma m_{0e} \mathbf{v}$ , with  $\gamma$  the relativistic gamma, and  $m_{0e}$  the electron rest mass);  
 402 pitch angle  $\alpha = \tan^{-1}(|p_{\perp}/p_{\parallel}|)$  (for  $p_{\perp}$  and  $p_{\parallel}$  the momenta perpendicular and parallel  
 403 to the background magnetic field); and  $L^* \propto 1/\Phi$ , is a value inversely proportional to the  
 404 third adiabatic invariant [Roederer and Zhang, 2013; Roederer and Lejosne, 2018]. The  
 405 work in this paper does not consider radial diffusion (i.e. diffusion in  $L^*$ ). It is the diffu-  
 406 sion in pitch angle, characterized by  $D_{\alpha\alpha} = D_{\alpha\alpha}(E, \alpha)$ , that will be the focus.

407 Particles are considered to be in resonance with a given wave mode when the wave-  
 408 particle resonance condition is satisfied [Kennel and Engelmann, 1966],

$$\omega - k_{\parallel} v_{\parallel} = n\omega_{ce}/\gamma. \quad (4)$$



356 **Figure 4.** ‘Dispersion relation’ of the  $B_y$  component of the waves present in the numerical experiment,  
 357 averaged over the entire spatial and temporal domain during the wave-particle interaction. The over-plotted  
 358 cyan curve marks the cold plasma dispersion relation (see equation (1)).

409 In this equation,  $\omega > 0$  is the wave frequency,  $n = 0, \pm 1, \pm 2, \dots$ ;  $k_{\parallel} = \mathbf{k} \cdot \mathbf{B}_0/B_0$  and  
 410  $v_{\parallel} = p_{\parallel}/(m_0e\gamma)$  are the wave vector and velocity components that are parallel to  $B_0$ , and  
 411 we remind that  $\omega_{ce} < 0$ . In the case of field-aligned whistler mode waves, only the  $n = -1$   
 412 resonance can occur for electrons (e.g. see *Summers* [2005]). Under these circumstances,  
 413 wave-particle resonance occurs for a given wave frequency,  $\omega$ , for pitch angles and ener-  
 414 gies defined by

$$\alpha = \cos^{-1} \left( \left| \frac{|\omega_{ce}|/\omega - (1 + \varepsilon)}{(kc/\omega)\sqrt{\varepsilon^2 + 2\varepsilon}} \right| \right), \quad (5)$$

415 for  $\varepsilon = E/(m_0ec^2)$ , and  $kc/\omega$  given by equation (1). This equation implies that for a given  
 416 pitch angle, lower frequency waves resonate with higher energies [*Camporeale*, 2015;  
 417 *Chen et al.*, 2018]. Furthermore, for a given wave frequency, the values of particle energy  
 418 that can resonate are a monotonically increasing function of pitch angle.

### 419 3.1 Background theory on normal diffusion

420 An implicit assumption in the use of QLT is that the plasma undergoes ‘normal dif-  
 421 fusion’ [*Bouchaud and Georges*, 1990] in phase-space: “the diffusion model assumes the  
 422 existence of an underlying uncorrelated, Gaussian stochastic process, i.e., a Brownian ran-  
 423 dom walk” [*del Castillo-Negrete et al.*, 2004]. In this normal diffusive framework, diffusion  
 424 coefficients are defined by the following formula (for arbitrary variables  $X$  and  $Y$ ),

$$D_{XY}(X, Y) = \frac{\langle \Delta X_l \rangle \langle \Delta Y_l \rangle}{2\Delta t}, \quad (6)$$

425 in units of  $[X][Y]s^{-1}$ . Here,  $\Delta t$  is interpreted as the duration over which the diffusion co-  
 426 efficients are to be calculated,  $X_l$  and  $Y_l$  are distributions of the particle parameters, lo-  
 427 calized to given values of  $X$  and  $Y$  (for  $N$  particles  $l = 1, 2, \dots, N$  within the given local  
 428 population). The mean of the distribution  $X_l$  is denoted by  $\langle X_l \rangle$ , and

$$\langle \Delta X_l \rangle \equiv \langle X_l - \langle X_l \rangle \rangle, \quad (7)$$

429 such that  $\langle \Delta X_l \rangle^2 \equiv \text{var}(X_l)$ , for  $\text{var}(X_l)$  the variance of the distribution  $X_l$ . Implicit within  
 430 this normal diffusion construction, is that the variance of a given parameter scales linearly

with time,

$$\Delta\text{var}(X_l) = 2D_{XX}\Delta t, \quad (8)$$

for  $\Delta\text{var}(X_l)$  the change in the variance of  $X_l$  over the time  $\Delta t$  (e.g. see *Bouchaud and Georges* [1990]; *Metzler and Klafter* [2000]). Conceptually, this means that for a given subset of a plasma population that is located in some region of phase space, then the distribution of that subset will spread in phase space according to equation (8).

#### 4 Diffusion in our numerical experiments

Particle diffusion due to wave-particle interactions is monitored by using the EPOCH ‘tracer’ particle feature. EPOCH allows the embedding of test-particle populations (tracers) into numerical experiment. Unlike all the other particle populations, tracer particles do not contribute to the current, and so they effectively act as labels in phase-space: that is to say that the behaviour of a given tracer is indicative of the behaviour of an interacting particle (one that does contribute moments) in the same given region of phase-space. We release  $\approx 10^8$  tracer particles within the domain at  $t = 0$ , that are initially distributed according to a 100keV Maxwellian distribution that is uniform in space. Since they do not contribute current, we can load tracers however we want in phase space. We choose this specific ‘temperature’ merely to provide a relatively uniform distribution of particles across the section of energy space important for pitch-angle diffusion in the Radiation Belts.

Once the driven wave profile crosses the experimental domain, we consider all of the tracer particles to be under the influence of the whistler-mode waves. At  $t = t_{\text{cross}}$ , we bin the tracer particles in two dimensions according to their values of energy and pitch angle at that time. We emphasize that tracers then remain identified with that given bin for the entirety of the experiment, i.e. we do not re-bin at each data-dump. The binning process is performed as follows. We first order all of the  $\approx 10^8$  tracers according to their energy at  $t = t_{\text{cross}}$ , and separate these tracers into 250 intervals, which are defined so as to allow exactly identical numbers of tracers in each interval. Within each of these energy intervals, the tracers are then ordered according to their value of pitch angle, and subdivided into 90 pitch angle sub-intervals, defined in order to allow the same number of tracers in each. Each of these  $250 \times 90$  bins in energy and pitch-angle space contains 4444 tracer particles, and therefore we have uniformly good statistics within each bin with which to calculate the diffusive response. In the case of an isotropic Maxwellian distribution, it would be expected that this procedure would yield bins of a uniform size in pitch angle space, within each energy interval. Our bins are not exactly uniform in pitch angle space, but they are almost uniform. The reason is as follows. The tracer particles are loaded into the simulation at  $t = 0$  as an isotropic Maxwellian. However, they are binned at a later time,  $t = t_{\text{cross}}$ . Between  $t = 0$  and  $t = t_{\text{cross}}$ , the tracers have been responding to the electromagnetic perturbations within the domain created by both the wave excitation mechanism and any other inherent PiC electromagnetic fluctuations, and therefore the tracers are not in a perfectly isotropic state at  $t = t_{\text{cross}}$ .

##### 4.1 Scattering in phase-space

Figure 5 shows an example of the diffusive response for particles within a bin roughly centred on  $\alpha = 75^\circ$  and  $E = 50\text{keV}$ . This combination of energy and pitch angle implies that the particles are in resonance with the driven wave spectrum. From hereon in we redefine  $t = t_{\text{cross}}$  as  $\tilde{t} = 0$ , and the end of the simulation as  $\tilde{t} = T$ , to simplify the discussion. Figures 5(a)-(d) plot electron  $E, \alpha$  values at  $\tilde{t} = 0, T/3, 2T/3$  and  $\tilde{t} = T$  respectively, and figures 5(e)-(h) plot pitch angle distributions of the entire sub-population (all energies). It is evident that pitch-angle diffusion dominates over energy diffusion in this bin, for reasoning as follows. The maximum magnitude of the pitch angle scattering in this bin reaches values of  $(\max(\Delta\alpha))^2/(2T) \approx (\pm 3)^2/(2T) = 9/(2T)$ . Whereas the en-

480 ergy scattering in this bin reaches maximum magnitudes of  $(1/E^2)(\max(\Delta E))^2/(2T) \approx$   
 481  $(1/50\text{keV})^2(\pm 1\text{keV})^2/(2T) = 0.0004/(2T)$ . We have checked that the dominance of pitch-  
 482 angle scattering is observed in most bins. This is an expected result, since the ratio  $f_{pe}/f_{ce}$   
 483 is known to control the relative significance of energy versus pitch angle diffusion [Sum-  
 484 mers, 2005]. It is also interesting to note that the particles are scattered in preferred di-  
 485 rections. This scattering is such that positive changes in  $E$  correlate with positive changes  
 486 in  $\alpha$ , and negative changes in  $E$  correlate with negative changes in  $\alpha$ . We have observed  
 487 that this behaviour is ubiquitous for the particles that are in resonance with the dominant  
 488 whistler-mode waves, and therefore the particles which undergo ‘significant diffusion’ (see  
 489 section 4.3 for a discussion on this topic, and our definition of ‘significant diffusion’). The  
 490 observed scattering in a preferred direction is an expected result due to the following argu-  
 491 ment. During a resonant interaction with a given parallel-propagating whistler-mode wave  
 492 ( $\omega_k < |\omega_{ce}|$ ), then (in the rest frame of the wave) an electron will experience changes in  
 493 the total kinetic energy,  $\Delta E$ , and the perpendicular kinetic energy,  $\Delta E_{\perp}$ , that are related  
 494 according to

$$\Delta E_{\perp}/\Delta E = |\omega_{ce}|/\omega_k > 1, \quad (9)$$

495 (e.g. see equation (36) in *Brice* [1964]). Equation (9) implies that (in the rest frame of the  
 496 wave) for a given positive change in the electron energy ( $\Delta E > 0$ ), such that

$$\Delta E = \Delta E_{\perp} + \Delta E_{\parallel},$$

497 then the perpendicular energy must increase by a greater amount, i.e.  $\Delta E_{\perp} > \Delta E$ . There-  
 498 fore the parallel energy must decrease ( $\Delta E_{\parallel} < 0$ ). This therefore implies that the pitch  
 499 angle must increase. One can use an exactly analogous argument using equation (9) to  
 500 conclude that a decrease in the energy of an electron ( $\Delta E < 0$ ) is consistent with a de-  
 501 crease of the electron pitch angle. These, and other, helpful observations are summarized  
 502 in Table 1. of *Brice* [1964], and can also be seen clearly in Figure 1. from *Kennel and*  
 503 *Petschek* [1966].

504 Furthermore, we see from Figure 5 that the particle population spreads from an ini-  
 505 tial ‘top-hat’ sample, into a Gaussian-type distribution. This property seems broadly con-  
 506 sistent with the diffusive paradigm, in which initially localized distributions spread into  
 507 Gaussian distributions with ever greater widths (variances).

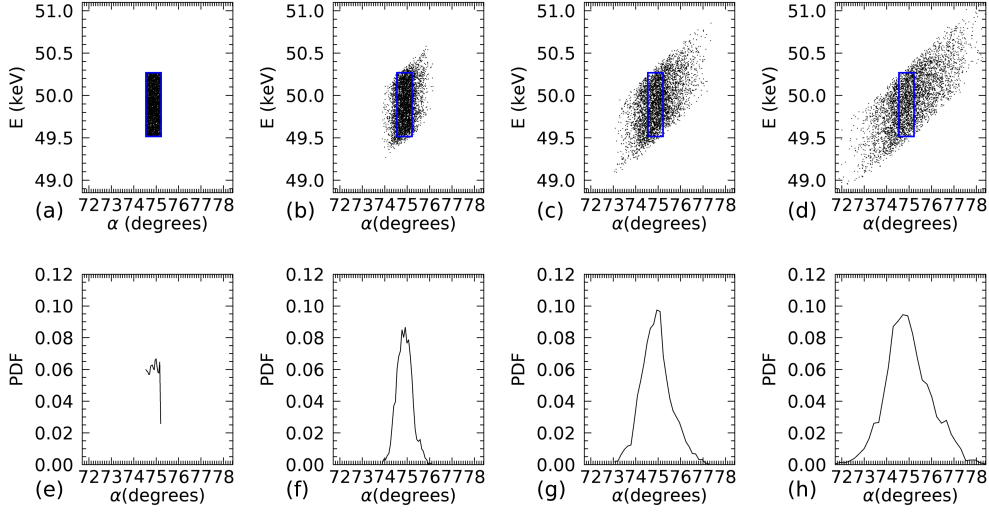
## 511 4.2 The diffusive hypothesis

512 The direct evaluation of the nature of diffusion in response to a given wave spec-  
 513 trum, relies on both the plasma and wave characteristics being quasi-static for the time  
 514 considered,  $\Delta t$  [*Schulz and Lanzerotti*, 1974]. Further to this requirement, we propose  
 515 some additional constraints that are described by the following hierarchy of timescales,

$$\tau_{\text{wave}} \ll \Delta t \leq \tau_{B(\omega,k)}, \tau_{n,B_0}, \tau_{\text{local}}, \quad (10)$$

516 that should be satisfied in order for one to directly measure properties of the diffusion for  
 517 a given  $(E, \alpha)$  bin. Equation (10) states that one can meaningfully evaluate diffusion due  
 518 to interactions with a given wave frequency over timescales: (i) significantly larger than  
 519  $\tau_{\text{wave}} = 1/f_{\text{wave}}$ ; (ii) smaller than those for which one observes variations in the wave spec-  
 520 trum ( $\tau_{B(\omega,k)}$ ); (iii) and smaller than those for which one observes variations in the the  
 521 background magnetic field and number density ( $\tau_{n,B_0}$ ). These conditions hold for our ex-  
 522 periment.

523 Furthermore, in order to be able to consider the rate of diffusion as a function of  $E$   
 524 and  $\alpha$  over some timescale  $\Delta t$ , each given sub-population (or bin) of particles must remain  
 525 localized to the same given region of  $(E, \alpha)$  space for the duration of  $\Delta t$ . To be clear, con-  
 526 sider one particular bin composed of  $l = 1, 2, \dots, N$  particles, with initial values binned



508 **Figure 5.** The diffusive response for 4444 electrons, within a bin roughly centred on  $75^\circ$  and 50keV. (a)-(d)  
 509 plot electron  $E, \alpha$  values at  $\tilde{t} = 0, T/3, 2T/3$  and  $\tilde{t} = T$  respectively. (e)-(h) plot pitch angle distributions of  
 510 the given particles at those times.

527 according to  $[(E_{\text{bin, min}} < E_l(t=0) < E_{\text{bin, max}}), (\alpha_{\text{bin, min}} < \alpha_l(t=0) < \alpha_{\text{bin, max}})]$ . Then, in  
 528 order to be able to measure diffusion for that given bin, we require

$$\begin{aligned} E_{\text{bin, min}} < \langle E_l \rangle(\tilde{t}) < E_{\text{bin, max}}, \\ \alpha_{\text{bin, min}} < \langle \alpha_l \rangle(\tilde{t}) < \alpha_{\text{bin, max}}. \end{aligned} \quad (11)$$

529 We define the timescale over which  $\langle E_l \rangle(t)$  and  $\langle \alpha_l \rangle(\tilde{t})$  satisfy the above constraints  
 530 in a given bin as  $\tau_{\text{local}}$ . Therefore, if satisfied, then the electrons in the given bin undergo  
 531 negligible advection in  $(E, \alpha)$  space over the timescale  $\tau_{\text{local}}$ .

532 Figure (6) plots a normalized measure of local advection in phase-space,

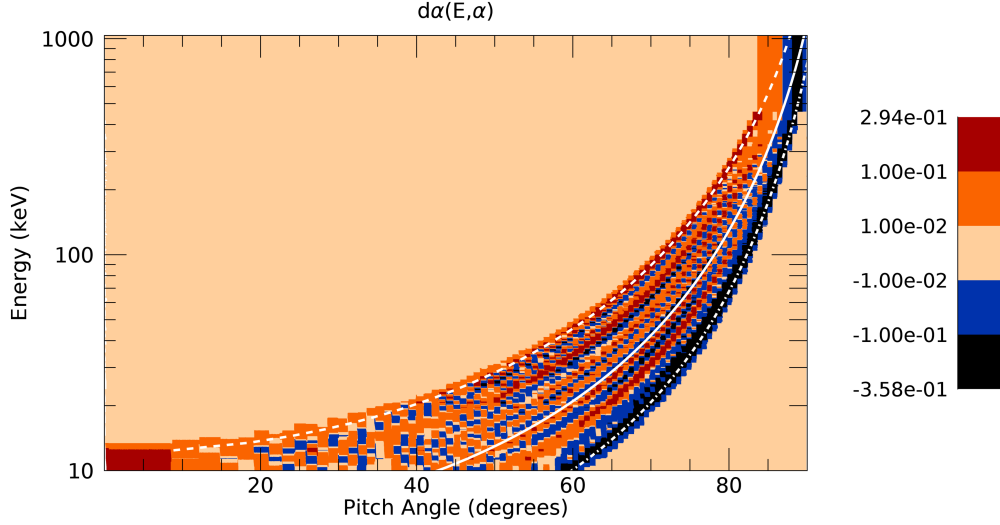
$$d\alpha(E, \alpha) := \frac{\Delta \langle \alpha_l \rangle}{|\text{bin}(\alpha_l)|}. \quad (12)$$

533 Here,  $\Delta \langle \alpha_l \rangle = \langle \alpha_l \rangle(\tilde{t} = T) - \langle \alpha_l \rangle(\tilde{t} = 0)$ , and  $|\text{bin}(\alpha)| = \alpha_{\text{bin, max}} - \alpha_{\text{bin, min}}$ . The  
 534 over-plotted white curves mark the values of energy and pitch angle that are (according  
 535 to equations (4) and (5)) in “ $n = -1$  resonance” with waves of frequency  $f_{lc}$  (‘dash’),  $f_{uc}$   
 536 (‘dash-dot’), and  $(f_{lc} + f_{uc})/2$  (‘solid’). We can see that the largest values of  $d\alpha$  are lo-  
 537 calized to regions within the boundaries of the resonance curves, and have maximum size  
 538 less than 0.5 ( $\max(|d\alpha|) \approx 0.36$ ). Therefore, for this choice of binning, all electron sub-  
 539 populations remain localized to their given pitch-angle bins for the duration of the interac-  
 540 tion that we consider,  $0 < \tilde{t} < T$ . Therefore an evaluation of diffusive properties is valid,  
 541 i.e. timescales are in agreement with equation (10) and the diffusive hypothesis holds over  
 542 the given timescale  $\Delta t = 460t_{ce}$ . We have also constructed a similar plot for  $dE$ , which  
 543 shows qualitatively similar results ( $\max(|dE|) \approx 0.25$ ), and so sub-populations also remain  
 544 localized to their given energy bins.

### 548 4.3 Nature of the diffusion

549 As described at the beginning of Section 3, the calculation of a diffusion coefficient  
 550 (e.g.  $D_{\alpha\alpha}$ ) within the normal diffusive paradigm assumes that the variances of electron





545 **Figure 6.**  $d\alpha(E, \alpha)$ , for each  $(E, \alpha)$  bin in the experiment (see equation (12)). The over-plotted white curves  
 546 mark the values of energy and pitch angle that are (according to equations (4) and (5)) in “ $n = -1$  resonance”  
 547 with waves of frequency  $f_{lc}$  (‘dash’),  $f_{uc}$  (‘dash-dot’), and  $0.5(f_{lc} + f_{uc})$  (‘solid’).

551 pitch-angle distributions within a given bin grow linearly with time. In this case, the dif-  
 552 fusion coefficient is given by equation (8), and defines the slope of the line according to  
 553  $\text{var}(\alpha_l) = 2D_{\alpha\alpha}\Delta t$ . Prior to calculating diffusion coefficients, it is therefore important to  
 554 check whether the data supports this implicit assumption of ‘variances that grow linearly  
 555 in time’.

559 Figures 7(a)-(c) plot the evolution of  $\text{var}(\alpha_l)$  for three different example bins. These  
 560 bins are given by  $(E, \alpha) = (20\text{keV}, 45^\circ)$  ( $300\text{keV}, 82^\circ$ ), and  $(50\text{keV}, 75^\circ)$ . The asterisks  
 561 mark the directly extracted particle data, and the solid black lines mark curve fits. The  
 562 curve-fitting method is described in Appendix B. For the purposes of presentation, the par-  
 563 ticle variance curves are translated so that  $\text{var}(\alpha_l; \tilde{t} = 0) = 0$ . An instantaneous measure  
 564 of the rate of diffusion could be considered to be  $d(\text{var}(\alpha_l))/d\tilde{t}$ . Figure 7(b) shows an ex-  
 565 ample for which this rate of diffusion appears to be roughly constant in time. However,  
 566 figures 7(a) and 7(c) show examples for which the rate appears, respectively, to be slowing  
 567 down and speeding up as time passes. This time-dependent rate of diffusion is an interest-  
 568 ing feature, and does not (at first glance) appear consistent with the assumptions of normal  
 569 diffusion theory. Diffusive theories that move beyond the assumption of normal diffusion  
 570 (sometimes called ‘anomalous diffusion’) have many applications, and not only in space  
 571 physics (e.g. see *Bouchaud and Georges* [1990]; *Metzler and Klafter* [2000]; *Zaslavsky*  
 572 [2002]; *Perrone et al.* [2013]; *Zimbardo et al.* [2015]). Anomalous diffusion theory essen-  
 573 tially allows for the variance of a given parameter  $X$  to evolve according to a power-law

$$\text{var}(X_l) \propto t^a, \quad (13)$$

574 for  $0 < a < \infty$ , and for which  $a < 1$  denotes ‘sub-diffusion’,  $a \approx 1$  denotes ‘normal  
 575 diffusion’, and  $a > 1$  denotes ‘super-diffusion’. Using this interpretation, figures 7(a)-(c)  
 576 present values  $a = 0.52$ ,  $a = 0.92$  and  $a = 2.21$  respectively (suggesting sub-, normal- and  
 577 super-diffusion respectively). It is interesting to see that the diffusion observed does not  
 578 always follow normal diffusive behaviour over the time-scales  $0 < \tilde{t} < T$ . Each sub-figure  
 579 also includes a blue solid line, obtained via imposing a linear fit to the raw data over the  
 580 second half of the wave-particle interaction,  $T/2 < \tilde{t} < T$ . These straight lines are a good

fit in each case. This suggests that normal diffusion is observed in all three cases, but only after an initial transient phase during which anomalous diffusion occurred.

Figure 8 plots the evolution of  $\text{var}(\alpha)$  for a bin roughly centred on  $(E, \alpha) = (9.2\text{keV}, 40^\circ)$ . This sub-population of particles is resonant with waves of frequency  $f = 0.3f_{ce}$ , and represents a direct comparison with the main example plotted by *Tao et al.* [2011] (figure 2 in that paper). The black and blue solid lines represent the same curve fits as applied to figure 7. The solid green line represents the theoretical evolution of  $\text{var}(\alpha)$ , as inferred by using the value of  $D_{\alpha\alpha}$  as predicted from the PADIE code [*Glauert and Horne, 2005*] using input plasma and wave parameters as detailed in this paper. As a reminder, note that  $\text{var}(\alpha) = 2\Delta t D_{\alpha\alpha}$  under the assumption of normal diffusion. The diffusion index for this bin is given by  $a = 1.15$  and therefore classified as normal diffusion. We see a very good agreement between the theoretical diffusion coefficient and our directly extracted data on the diffusive response for this particular energy and pitch-angle bin. We will follow up on direct comparisons between  $D_{\alpha\alpha}$  as predicted from the PADIE code and diffusive response in our PiC experiments in a separate paper that will include all energy and pitch-angle bins.

Figure 9 presents contour plots of the diffusion index,  $a$ , for each  $(E, \alpha)$  bin, as defined in equation (13). We remind that we calculate the value  $a$  for each and every bin over all phase space ( $0 < \alpha < 90$ ,  $9\text{keV} < E < 1\text{MeV}$ ). The rate of diffusion that is observed is a function of phase-space, and we observe very weak diffusion in some bins. We do not present the value of  $a$  when diffusion is very weak, and instead mask those cases with black. For this purpose, a measure of the strength of the diffusion is calculated as follows. We calculate the total change in the variance of the pitch-angle distributions within each bin,

$$D_{\alpha\alpha,\text{proxy}}(E, \alpha) = \frac{\text{var}(\alpha_I; \tilde{t} = T) - \text{var}(\alpha_I; \tilde{t} = 0)}{2T}. \quad (14)$$

Significant diffusion is deemed to have occurred within a given bin, if the value of this diffusion proxy satisfies

$$D_{\alpha\alpha,\text{proxy}}(E, \alpha) > 10^{-2} \max_{E, \alpha} \{D_{\alpha\alpha,\text{proxy}}(E, \alpha)\}. \quad (15)$$

If significant diffusion does occur, then we describe its nature as ‘sub-diffusion’ if  $a < 0.67$  by using yellow, as normal diffusion if  $0.67 < a < 1.5$  by using pink, or as ‘super-diffusion’ if  $a > 1.5$  by using dark-red. These bounds of  $a < a_{\text{sub}} = 2/3$  and  $a > a_{\text{super}} = 1/a_{\text{sub}}$  were chosen in order to classify sub- and super-diffusion relatively strictly. Any regions for which the curve-fitting routine failed, are represented by missing data (white). As was done for figure 6, the over-plotted cyan curves mark the values of energy and pitch angle that are in “ $n = -1$  resonance” with the driven waves. Furthermore, the locations of the bins represented in figure 7(a)-(c) are marked by cyan symbols: “<”, “★” and “>” respectively. Figure 9(a) shows the value of  $a$  that is calculated over the entire wave-particle interaction ( $0 < t < T$ ). One clear observation is that the regions of significant diffusion, as defined by equation (15), are almost exclusively localized within the “ $n = -1$  resonance” regions of phase space. Figure 9(a) also shows two well-defined region of sub- and super-diffusive behaviour. The sub-diffusive region is found at ‘lower-frequency’ resonances, and predominantly lower energies ( $< 100\text{keV}$ ); whereas the super-diffusive behavior is observed for ‘higher-frequency’ resonances, and across the entire energy range. Out of all bins in which significant diffusion was observed, 7.2% show sub-diffusion, 45% show normal-diffusion, and 47.8% show super-diffusion.

Figure 9(b) shows the same quantity as figure 9(a), but calculated over the second-half of the interaction ( $T/2 < \tilde{t} < T$ ). This plot is motivated by the hypothesis made after analysis of figures 7(a)-(c), that an initial transient period of varying diffusion rates gives way to normal diffusion in the latter half of the experiment. We indeed see from figure 9(b) that a smaller proportion of the plot (i.e. fewer bins) displays the sub- and super-diffusive behaviour. This observation is consistent with the observations made of the data

in figures 7(a)-(c): during  $0 < \tilde{t} < T/2$  we observe an initial transient phase during which different kinds of diffusive responses are possible; later on (during  $T/2 < \tilde{t} < T$ ) we observe a shift towards a normal-diffusive response. Out of all bins in which meaningful diffusion was observed, 2.9% show sub-diffusion, 86.7% show normal-diffusion, and 10.4% show super-diffusion during the second half of the numerical experiment.

## 5 Discussion

We use the EPOCH particle-in-cell code [Arber *et al.*, 2015] to track electron pitch-angle diffusion due to interactions with whistler-mode waves. There are two main novel features to our approach: (i) we consider diffusion using a PiC code as a boundary value problem, i.e. we excite specific wave modes at the boundary, as opposed to considering an initial-value problem in which one typically considers waves that grow from an initially unstable distribution (e.g. see *Katoh and Omura* [2006]; *Omura et al.*; *Hikishima et al.* [2009]; *Omura et al.* [2009]; *Omidi et al.* [2010, 2011]; *Katoh and Omura* [2013]; *Camporeale* [2015]; *Camporeale and Zimbardo* [2015]; *Silva et al.* [2017]; *Ratcliffe and Watt* [2017]; *Katoh et al.* [2018]); (ii) by considering the response of a distribution of electrons, we track the diffusion in energy and pitch angle space across the entire phase-space domain, in contrast to some previous similar studies of diffusion (e.g. see *Tao et al.* [2011, 2012a]; *Camporeale and Zimbardo* [2015]) that considered resonant particles only. These novel features allow us to, respectively: (i) consider a ‘quasi-static’ system, in which the background plasma and whistler-mode wave spectra are roughly time-independent; (ii) derive characteristics of the diffusive response for all electrons, including those that are non-resonant with the waves and typically not expected to strongly interact.

In this first study, we model the background plasma as a 0.1eV isotropic cold population. We use this approach to benchmark our novel method with expected results, before studying more realistic ‘radiation belt’ background plasmas in the future, with ‘warm’ and ‘hot’ anisotropic electron populations (see e.g. *Denton et al.* [2010]). We also make the assumption of spatially 1D dynamics, thereby permitting only parallel and anti-parallel wave propagation, as well as a homogeneous background magnetic field. This considerable simplification is done in order to benchmark with previous work [Tao *et al.*, 2011], and with a mind to a systematic future program of work with more realistic magnetic field geometries, wave-normal-angle spectra, and/or more ‘exotic’ wave modes and amplitudes. In order to properly understand each effect, it is necessary to first understand the experimental response in the most simple of circumstances, and then implement additions in isolation. We have compared our results for pitch angle diffusion with the example presented by *Tao et al.* [2011], using results from the PADIE code, and we see very good agreement. A more comprehensive comparison of the diffusive response with the predictions of QLT is beyond the scope of this paper, but will be addressed explicitly in future papers in this series.

Extremely low levels of background noise have been enabled by using the  $\delta F$  mode in EPOCH. This, in addition to the linear envelope applied to the wave driver, allows for a highly effective wave-driving mechanism for whistler-mode waves, with an excellent signal-noise-ratio. We have verified that the wave power is well localized to follow the cold plasma dispersion relation. A large number of tracer particles were embedded within the PiC domain ( $\approx 10^8$  electrons) by using the EPOCH tracer functionality. This provides good statistics with which we characterize the electron diffusion over the entire energy and pitch angle domain. The dominant diffusion is clearly seen to correspond to those particles that are in ‘ $n = -1$ ’ resonance with the driven wave mode, as expected by QLT. Diffusive effects outside the resonant regions of phase-space are at most 1% as significant as the dominant resonant effects. Therefore, for this experiment, non-resonant interactions are of little importance (unlike in e.g. *Camporeale* [2015]). This feature is an explicit requirement of QLT, and seems sensible given the simplified nature of the experimental setup.

692 Future investigations will seek to determine those circumstances under which nonlinear  
693 effects become more important.

694 One interesting feature of the diffusion is observed for early times; namely, a time-  
695 dependent rate of diffusion. The variances of pitch-angle distributions of given electron  
696 sub-populations do not always grow linearly with time during the first half of the experi-  
697 ment (see figures 7 and 9). We discuss this result in the context of ‘anomalous’ diffusion  
698 theories (e.g. see *Bouchaud and Georges* [1990]; *Metzler and Klafter* [2000]; *Zaslavsky*  
699 [2002]; *del Castillo-Negrete et al.* [2004]; *Perrone et al.* [2013]; *Zimbardo et al.* [2015]),  
700 that are known to play a role in various space and astrophysical plasma contexts. How-  
701 ever, at later times, normal diffusion (Brownian motion) is seen to dominate, during which  
702 time the variances grow with a linear rate. This latter result is consistent with the implicit  
703 assumptions of QLT, and suggests that in order to construct meaningful diffusion coeffi-  
704 cients from such PIC experiments, one may have to consider how to appropriately treat  
705 this initial transient phase (see examples of possible methods to treat time-dependent diffu-  
706 sion rates in e.g. *Degeling et al.* [2007]).

## 707 6 Summary

708 In this first paper of a series, we analyze the nature of the electron pitch-angle dif-  
709 fusion due to interactions with broadband and incoherent whistler-mode waves. The most  
710 significant technical development is a proof-of-concept for the novel method used. Namely,  
711 an analysis of the nature of electron diffusion over all phase-space due to specified whistler-  
712 wave modes, using a particle-in-cell method to construct a boundary-value problem. This  
713 analysis is enabled by direct extraction of particle data from numerical experiments per-  
714 formed using the EPOCH code. The numerical experiment was intended to both resemble  
715 and build upon the test-particle experiments performed by *Tao et al.* [2011]. As such, we  
716 drove an incoherent spectrum of whistler-mode waves into a simple cold plasma with uni-  
717 form background magnetic field, and tracked the diffusive response of  $\approx 10^8$  electrons for  
718  $460t_{ce}$ , as a function of energy and pitch angle. We make the following observations of  
719 our experiments:

- 720 1. The strength of the diffusive response is found to be a function of energy and pitch  
721 angle, as is expected using quasilinear diffusion theory. The diffusion is strongest  
722 in regions of energy-pitch angle space that are in the  $n = -1$  resonance with the  
723 dominant wave signal. This is not a new result, but a required one, since the only  
724 wave-particle resonance that is possible in our experiment is the  $n = -1$  case. How-  
725 ever, it is an important benchmarking criteria that our novel method must satisfy,  
726 and therefore it is important to check and present.
- 727 2. Non-resonant interactions are observed to be of little consequence in this case. This  
728 feature is directly observed in our numerical experiments, and is not *a priori* as-  
729 sumed. It will be interesting to check how this feature changes in future experi-  
730 ments.
- 731 3. When considered over the entire duration of the wave particle interaction for partic-  
732 ular regions of energy-pitch angle space, the nature of the diffusive response is ob-  
733 served in some regions of phase-space to be: (a) ‘normal’, i.e. it is Einsteinian/Brownian  
734 (for which the variances of energy or pitch angle grow linearly with time, as is im-  
735 plicit in QLT); (b) or ‘anomalous’, i.e. it is either super- or sub-diffusive (for which  
736 the variances of energy or pitch angle grow at either a faster or slower relative rate,  
737 respectively)
- 738 4. When considered over the second half of the wave-particle interaction, we observe  
739 that a larger proportion of phase-space exhibits a normal diffusive response due to  
740 the wave-particle interaction

- 741 5. A preliminary analysis of the strength of pitch-angle diffusion for a given region of  
 742 energy and pitch angle space demonstrates consistency with the results presented by  
 743 *Tao et al.* [2011], and the results of the PADIE code.

744 The results presented in this paper effectively benchmark our techniques against  
 745 other treatments that consider the response of test-particles to whistler-mode waves (e.g.  
 746 see *Tao et al.* [2011]). This work motivates the following future investigations on: (i) the  
 747 strength and nature of diffusion as a function of driving wave amplitude; (ii) the differ-  
 748 ence in the plasma response when more realistic radiation belt plasmas are modelled, i.e.  
 749 those with the fractional warm components that can be found in Earth’s inner magneto-  
 750 sphere. It will also be interesting to consider methods that allow for a analysis of a fully  
 751 self-consistent electron response to whistler-mode waves, i.e. to move beyond the mixed  
 752 ‘PiC – test-particle approach’ that we employed in this paper, and therefore beyond any of  
 753 its inherent limitations.

754 Beyond that, there are many questions remaining that motivate other future studies.  
 755 Namely, how do the results presented in this paper change when modelling other mani-  
 756 festations of whistler-mode waves (e.g. monochromatic waves), other wave spectra (e.g.  
 757 with a much wider wave-normal angle spectrum). It will also be important to study the  
 758 diffusive response in spatially two-dimensional plasmas, with both homogeneous and inho-  
 759 mogeneous background magnetic fields. Oblique waves can only propagate in a numerical  
 760 experiment that has more than one spatial dimension, and are known to be relevant for  
 761 some properties of whistler-mode wave dynamics in the radiation belts (e.g. see *Artemyev*  
 762 *et al.* [2016a]; *Ratcliffe and Watt* [2017]). All of these effects should be expected to pro-  
 763 duce qualitatively different diffusive responses.

## 764 A: The EPOCH particle-in-cell code

765 We use version 4.16 of the Extendable PiC Open Collaboration (EPOCH) code in  
 766 one spatial dimension (‘EPOCH1D’). EPOCH is an explicit [*Birdsall and Langdon*, 2004],  
 767 relativistic and charge-conserving PiC code [*Arber et al.*, 2015], using Villasenor and  
 768 Buneman current deposition [*Villasenor and Buneman*, 1992]. EPOCH solves Maxwell’s  
 769 equations combined with the equations of motion for charged particles in an EM field to  
 770 provide a direct simulation of collisionless plasma. Since EPOCH uses an explicit scheme,  
 771 numerical stability requirements dictate that timesteps,  $\Delta t$ , are limited by the usual CFL  
 772 condition, and the resolution of electron plasma waves, for a given grid discretization  $\Delta x$ .  
 773 EPOCH1D therefore sets the time scale as the most restrictive of constraints set by: the  
 774 CFL condition ( $\Delta t_{\text{CFL}} = \Delta x/c$ ); the inverse plasma frequency, (at the beginning of the  
 775 simulation); and the inverse ‘laser’ frequency (the term ‘laser’ refers to an electromagnetic  
 776 wave driver), according to

$$\Delta t < \min(\Delta t_{\text{CFL}}, 1/(2f_{\text{BG}}), 1/(2f_{\text{laser}})), \quad (\text{A.1})$$

777 for  $f_{\text{BG}} = |\omega_{\text{BG}}/(2\pi)|$  the ordinary frequency according to the Bohm-Gross dispersion  
 778 relation [*Bohm and Gross*, 1949], and  $f_{\text{laser}}$  the minimum laser frequency. All quantities in  
 779 EPOCH are given in normal SI units.

780 EPOCH allows users to run in ‘ $\delta F$  mode’. In general terms, if we consider a plasma  
 781 population as being described by a distribution function of the form  $F = F_0(\mathbf{x}, \mathbf{v}) + \delta F(\mathbf{x}, \mathbf{v}, t)$   
 782 (with  $F_0$  either an isotropic or anisotropic Maxwellian distribution function), then the  
 783  $\delta F$  method (e.g. see *Sydora* [1999]) can achieve a reduction in PiC noise of the order of  
 784  $\sim |\delta F|/F$ , for all other settings left unchanged. Hence, this method is particularly useful if  
 785  $F$  is close to an (an-)isotropic Maxwellian distribution function.

786 Instructions on how to download and run EPOCH are given in supplementary infor-  
 787 mation (S1).

## B: Curve-fitting procedure

Here we describe the curve-fitting procedure, used to determine the diffusion index  $a$ , as shown in figures 7, 8 and 9. In each  $(E, \alpha)$  bin, a time-series of the quantity

$$V_\alpha(\tilde{t}) = \frac{\text{var}(\alpha_I; \tilde{t}) - \text{var}(\alpha_I; \tilde{t} = 0)}{\text{var}(\alpha_I; \tilde{t} = 0)}, \quad (\text{B.1})$$

is calculated. We track  $V_\alpha$  instead of just the variance, so that all time-series are ordinated according to similar scales, and are initialized at zero. This also helps with the curve-fitting procedure which is performed as follows:

(i) First, we test to see whether or not any ‘significant diffusion’ occurs in each bin, using the rule defined by equation (15). (ii) If significant diffusion occurred then curve-fitting of the time-series,  $V_\alpha$ , is implemented, to the test function,

$$y = c_0 + c_1 x^{c_2}.$$

For a given initial estimate of the vector  $\mathbf{c} = [c_0, c_1, c_2]$ , the standard curve-fitting routine uses a gradient-expansion least-squares method, and returns a successful result when the relative decrease in chi-squared is less than  $10^{-3}$  in a given iteration. The routine returns a fail if convergence is not reached after a large number of iterations, or if the chi-squared value increases without bounds. Note that we classify ‘successful’ outputs of the curve-fitting algorithm as ‘failures’ if  $c_2 > 10$ , in order to neglect spuriously high values. Finally, curve-fitting could only be considered a success if  $|y(x=0)/y(x=x_{\max})| < 0.5$ .

(iii) For each bin, we employ this curve fitting routine for 100 different initial guesses of  $\mathbf{c}$ , and record the output values of all ‘successful’ attempts. We then select the output vector that minimizes the mean deviation between the curve fit and the data. In theory, normal diffusion would give  $c_2 \approx 1$ , with the coefficient  $c_1$  directly proportional to  $D_{\alpha\alpha}$ , and  $c_0 = 0$ .

## Acknowledgments

The supporting information provides: (S1) basic instructions on how to run the same experiment that is presented in the main article; (S2) the contents of the input text file, used for the numerical experiment that is presented in the main article. This information will enable readers to locally generate the same experimental data as was considered in the main article.

This research was supported by the Natural Environment Research Council (NERC) Highlight Topic Grant #NE/P017274/1 (Rad-Sat). This work was in part funded by the UK EPSRC grants EP/G054950/1, EP/G056803/1, EP/G055165/1 and EP/ M022463/1. This work was in part performed using the Cambridge Service for Data Driven Discovery (CSD3), part of which is operated by the University of Cambridge Research Computing on behalf of the STFC DiRAC HPC Facility ([www.dirac.ac.uk](http://www.dirac.ac.uk)). The DiRAC component of CSD3 was funded by BEIS capital funding via STFC capital grants ST/P002307/1 and ST/R002452/1 and STFC operations grant ST/R00689X/1. DiRAC is part of the National e-Infrastructure. This work was in part performed using the Research Processing Service (Met-Cluster) and the Reading Academic Computing Cluster (RACC) at the University of Reading.

The authors acknowledge helpful conversations with M. Balikhin, A.W. Degeling, F. Effenberger, C. Forsyth, R.B. Horne, T. Neukirch, I.J. Rae and S. Troscheit.

## References

Albert, J. M. (2001), Comparison of pitch angle diffusion by turbulent and monochromatic whistler waves, *Journal of Geophysical Research: Space Physics*, 106(A5), 8477–8482, doi:10.1029/2000JA000304.

- 832 Albert, J. M. (2002), Nonlinear interaction of outer zone electrons with vlf waves, *Geo-*  
 833 *physical Research Letters*, 29(8), 116–1–116–3, doi:10.1029/2001GL013941.
- 834 Albert, J. M. (2010), Diffusion by one wave and by many waves, *Journal of Geophysical*  
 835 *Research: Space Physics*, 115(A3), doi:10.1029/2009JA014732.
- 836 Arber, T. D., K. Bennett, C. S. Brady, A. Lawrence-Douglas, M. G. Ramsay, N. J. Sir-  
 837 combe, P. Gillies, R. G. Evans, H. Schmitz, A. R. Bell, and C. P. Ridgers (2015), Con-  
 838 temporary particle-in-cell approach to laser-plasma modelling, *Plasma Physics and Con-*  
 839 *trolled Fusion*, 57(11), 1–26.
- 840 Artemyev, A., O. Agapitov, D. Mourenas, V. Krasnoselskikh, V. Shastun, and F. Mozer  
 841 (2016a), Oblique whistler-mode waves in the earth’s inner magnetosphere: Energy dis-  
 842 tribution, origins, and role in radiation belt dynamics, *Space Science Reviews*, 200(1),  
 843 261–355, doi:10.1007/s11214-016-0252-5.
- 844 Artemyev, A. V., A. I. Neishtadt, A. A. Vasiliev, and D. Mourenas (2016b), Kinetic equa-  
 845 tion for nonlinear resonant wave-particle interaction, *Physics of Plasmas*, 23(9), 090,701,  
 846 doi:10.1063/1.4962526.
- 847 Artemyev, A. V., A. I. Neishtadt, A. A. Vasiliev, and D. Mourenas (2017), Probabilistic  
 848 approach to nonlinear wave-particle resonant interaction, *Phys. Rev. E*, 95, 023,204, doi:  
 849 10.1103/PhysRevE.95.023204.
- 850 Artemyev, A. V., A. I. Neishtadt, A. A. Vasiliev, and D. Mourenas (2018), Long-  
 851 term evolution of electron distribution function due to nonlinear resonant interac-  
 852 tion with whistler mode waves, *Journal of Plasma Physics*, 84(2), 905840,206, doi:  
 853 10.1017/S0022377818000260.
- 854 Birdsall, C., and A. Langdon (2004), *Plasma Physics via Computer Simulation*, Series in  
 855 Plasma Physics and Fluid Dynamics, Taylor & Francis.
- 856 Bohm, D., and E. P. Gross (1949), Theory of plasma oscillations. a. origin of medium-like  
 857 behavior, *Phys. Rev.*, 75, 1851–1864, doi:10.1103/PhysRev.75.1851.
- 858 Bortnik, J., R. M. Thorne, and N. P. Meredith (2008a), The unexpected origin of plas-  
 859 maspheric hiss from discrete chorus emissions, *Nature*, 452(7183), 62–66, doi:  
 860 10.1038/nature06741.
- 861 Bortnik, J., R. M. Thorne, and U. S. Inan (2008b), Nonlinear interaction of energetic  
 862 electrons with large amplitude chorus, *Geophysical Research Letters*, 35(21), doi:  
 863 10.1029/2008GL035500.
- 864 Bouchaud, J.-P., and A. Georges (1990), Anomalous diffusion in disordered media: Statis-  
 865 tical mechanisms, models and physical applications, *Physics Reports*, 195(4), 127 – 293,  
 866 doi:https://doi.org/10.1016/0370-1573(90)90099-N.
- 867 Breneman, A., C. Cattell, J. Wygant, K. Kersten, L. B. Wilson, S. Schreiner, P. J. Kellogg,  
 868 and K. Goetz (2011), Large-amplitude transmitter-associated and lightning-associated  
 869 whistler waves in the earth’s inner plasmasphere at  $l < 2$ , *Journal of Geophysical Re-*  
 870 *search: Space Physics*, 116(A6), doi:10.1029/2010JA016288.
- 871 Brice, N. (1964), Fundamentals of very low frequency emission generation mech-  
 872 anisms, *Journal of Geophysical Research (1896-1977)*, 69(21), 4515–4522, doi:  
 873 10.1029/JZ069i021p04515.
- 874 Camporeale, E. (2015), Resonant and nonresonant whistlers-particle interaction  
 875 in the radiation belts, *Geophysical Research Letters*, 42(9), 3114–3121, doi:  
 876 10.1002/2015GL063874.
- 877 Camporeale, E., and G. Zimbardo (2015), Wave-particle interactions with parallel whistler  
 878 waves: Nonlinear and time-dependent effects revealed by particle-in-cell simulations,  
 879 *Physics of Plasmas*, 22(9), 092,104, doi:10.1063/1.4929853.
- 880 Cattell, C., J. R. Wygant, K. Goetz, K. Kersten, P. J. Kellogg, T. von Rosenvinge, S. D.  
 881 Bale, I. Roth, M. Temerin, M. K. Hudson, R. A. Mewaldt, M. Wiedenbeck, M. Maksimovic,  
 882 R. Ergun, M. Acuna, and C. T. Russell (2008), Discovery of very large ampli-  
 883 tude whistler-mode waves in earth’s radiation belts, *Geophysical Research Letters*, 35(1),  
 884 doi:10.1029/2007GL032009.

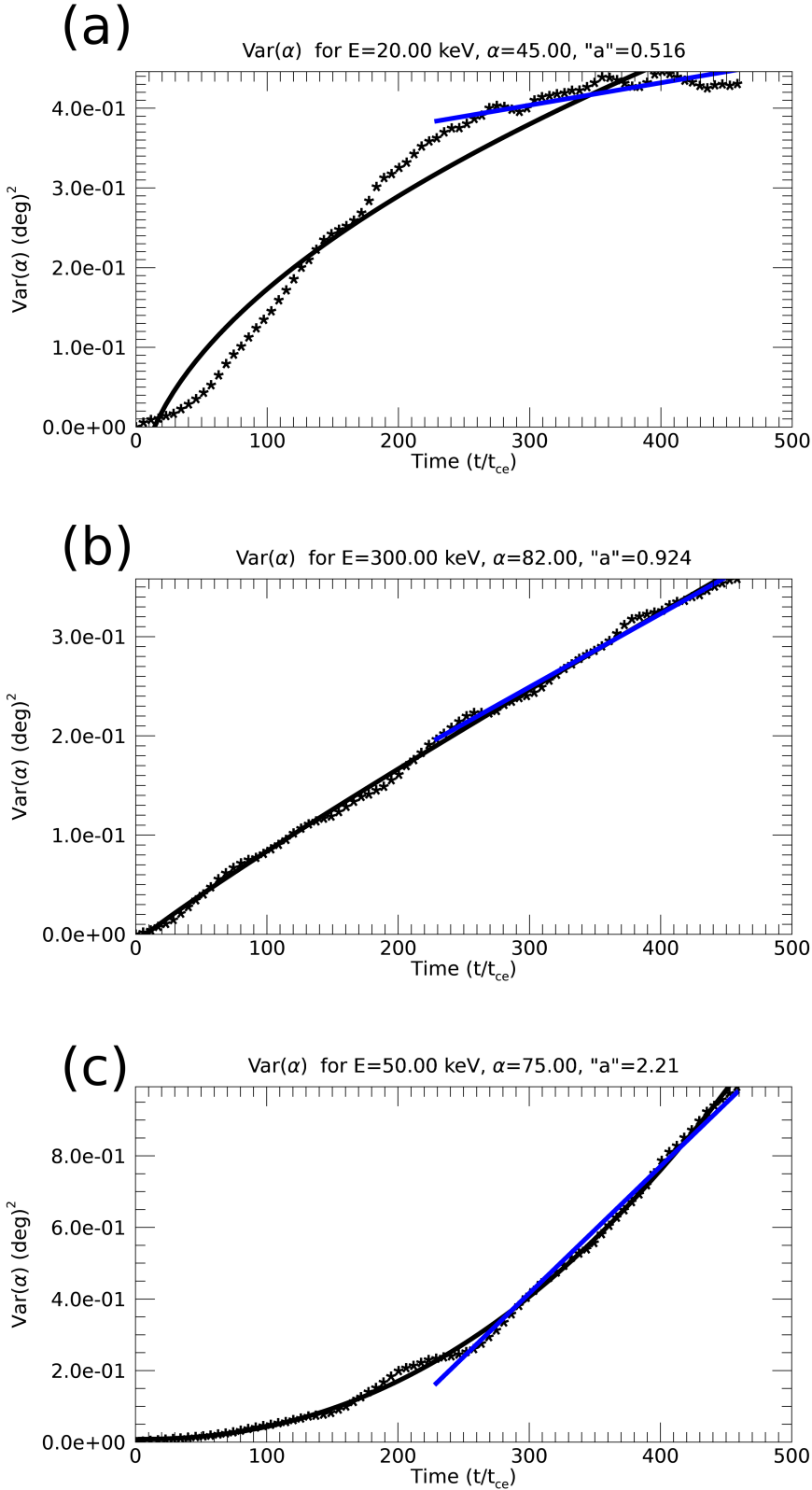
- 885 Chen, H., X. Gao, Q. Lu, Y. Ke, and S. Wang (2017), Lower band cascade of whistler  
886 waves excited by anisotropic hot electrons: One-dimensional pic simulations,  
887 *Journal of Geophysical Research: Space Physics*, 122(10), 10,448–10,457, doi:  
888 10.1002/2017JA024513.
- 889 Chen, H., X. Gao, Q. Lu, J. Sun, and S. Wang (2018), Nonlinear evolution of counter-  
890 propagating whistler mode waves excited by anisotropic electrons within the equatorial  
891 source region: 1-d pic simulations, *Journal of Geophysical Research: Space Physics*,  
892 123(2), 1200–1207, doi:10.1002/2017JA024850.
- 893 Chen, L., W. Li, J. Bortnik, and R. M. Thorne (2012), Amplification of whistler-  
894 mode hiss inside the plasmasphere, *Geophysical Research Letters*, 39(8), doi:  
895 10.1029/2012GL051488.
- 896 Chen, L., R. M. Thorne, J. Bortnik, W. Li, R. B. Horne, G. D. Reeves, C. A. Kletzing,  
897 W. S. Kurth, G. B. Hospodarsky, H. E. Spence, J. B. Blake, and J. F. Fennell (2014),  
898 Generation of unusually low frequency plasmaspheric hiss, *Geophysical Research Let-*  
899 *ters*, 41(16), 5702–5709, doi:10.1002/2014GL060628.
- 900 Cully, C. M., J. W. Bonnell, and R. E. Ergun (2008), Themis observations of long-lived  
901 regions of large-amplitude whistler waves in the inner magnetosphere, *Geophysical Re-*  
902 *search Letters*, 35(17), doi:10.1029/2008GL033643.
- 903 Degeling, A., R. Rankin, K. Kabin, R. Marchand, and I. Mann (2007), The effect of ulf  
904 compressional modes and field line resonances on relativistic electron dynamics, *Plane-*  
905 *tary and Space Science*, 55(6), 731 – 742, doi:https://doi.org/10.1016/j.pss.2006.04.039,  
906 ultra-Low Frequency Waves in the Magnetosphere.
- 907 del Castillo-Negrete, D., B. A. Carreras, and V. E. Lynch (2004), Fractional diffusion in  
908 plasma turbulence, *Physics of Plasmas*, 11(8), 3854–3864, doi:10.1063/1.1767097.
- 909 Denton, M. H., J. E. Borovsky, and T. E. Cayton (2010), A density-temperature descrip-  
910 tion of the outer electron radiation belt during geomagnetic storms, *Journal of Geophys-*  
911 *ical Research: Space Physics*, 115(A1), doi:10.1029/2009JA014183.
- 912 Fälthammar, C.-G. (1965), Effects of time-dependent electric fields on geomagneti-  
913 cally trapped radiation, *Journal of Geophysical Research*, 70(11), 2503–2516, doi:  
914 10.1029/JZ070i011p02503.
- 915 Gao, X., Q. Lu, J. Bortnik, W. Li, L. Chen, and S. Wang (2016), Generation of multiband  
916 chorus by lower band cascade in the earth’s magnetosphere, *Geophysical Research Let-*  
917 *ters*, 43(6), 2343–2350, doi:10.1002/2016GL068313.
- 918 Gao, X., Y. Ke, Q. Lu, L. Chen, and S. Wang (2017), Generation of multiband chorus  
919 in the earth’s magnetosphere: 1-d pic simulation, *Geophysical Research Letters*, 44(2),  
920 618–624, doi:10.1002/2016GL072251.
- 921 Glauert, S. A., and R. B. Horne (2005), Calculation of pitch angle and energy diffusion  
922 coefficients with the PADIE code, *Journal of Geophysical Research*, 110(A4), A04,206,  
923 doi:10.1029/2004JA010851.
- 924 Glauert, S. A., R. B. Horne, and N. P. Meredith (2014), Three-dimensional electron radi-  
925 ation belt simulations using the bas radiation belt model with new diffusion models for  
926 chorus, plasmaspheric hiss, and lightning-generated whistlers, *Journal of Geophysical*  
927 *Research: Space Physics*, 119(1), 268–289, doi:10.1002/2013JA019281.
- 928 Hikishima, M., S. Yagitani, Y. Omura, and I. Nagano (2009), Full particle simulation of  
929 whistler-mode rising chorus emissions in the magnetosphere, *JGR: Space Physics*.
- 930 Horne, R. B., R. M. Thorne, Y. Y. Shprits, N. P. Meredith, S. A. Glauert, A. J. Smith,  
931 S. G. Kanekal, D. N. Baker, M. J. Engebretson, J. L. Posch, M. Spasojevic, U. S. Inan,  
932 J. S. Pickett, and P. M. E. Decreau (2005a), Wave acceleration of electrons in the Van  
933 Allen radiation belts, *Nature*, 437, 227–230, doi:10.1038/nature03939.
- 934 Horne, R. B., R. M. Thorne, S. A. Glauert, J. M. Albert, N. P. Meredith, and R. R. An-  
935 derson (2005b), Timescale for radiation belt electron acceleration by whistler mode cho-  
936 rus waves, *JGR: Space Physics*, 110, A03225.
- 937 Hudson, M. K., S. R. Elkington, J. G. Lyon, and C. C. Goodrich (2000), Increase in rel-  
938 ativistic electron flux in the inner magnetosphere: ULF wave mode structure, *Advances*



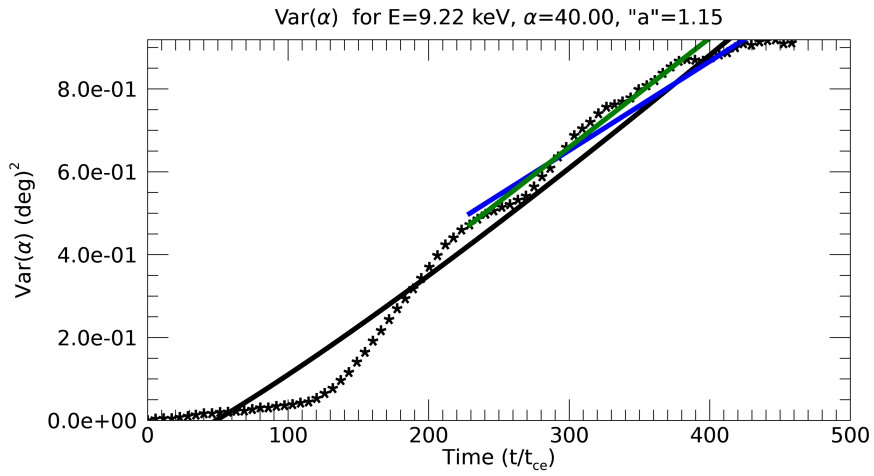
- 939 *in Space Research*, 25(12), 2327–2337, doi:10.1016/S0273-1177(99)00518-9.
- 940 Katoh, Y., and Y. Omura (2006), A study of generation mechanism of VLF triggered  
941 emission by self-consistent particle code, *JGR: Space Physics*, 111, A12207.
- 942 Katoh, Y., and Y. Omura (2013), Effect of the background magnetic field inhomogeneity  
943 on generation processes of whistler-mode chorus and broadband hiss-like emissions,  
944 *JGR: Space Physics*, 118, 4189–4198.
- 945 Katoh, Y., Y. Omura, Y. Miyake, H. Usui, and H. Nakashima (2018), Dependence of gen-  
946 eration of whistler mode chorus emissions on the temperature anisotropy and density of  
947 energetic electrons in the earth's inner magnetosphere, *Journal of Geophysical Research:*  
948 *Space Physics*, 123(2), 1165–1177, doi:10.1002/2017JA024801.
- 949 Kellogg, P. J., C. A. Cattell, K. Goetz, S. J. Monson, and L. B. Wilson (2011), Large am-  
950 plitude whistlers in the magnetosphere observed with wind-waves, *Journal of Geophys-  
951 ical Research: Space Physics*, 116(A9), doi:10.1029/2010JA015919.
- 952 Kennel, C. F., and F. Engelmann (1966), Velocity space diffusion from weak plasma  
953 turbulence in a magnetic field, *The Physics of Fluids*, 9(12), 2377–2388, doi:  
954 10.1063/1.1761629.
- 955 Kennel, C. F., and H. E. Petschek (1966), Limit on stably trapped particle fluxes, *Journal*  
956 *of Geophysical Research (1896-1977)*, 71(1), 1–28, doi:10.1029/JZ071i001p00001.
- 957 Langdon, A. (1970), Effects of the spatial grid in simulation plasmas, *Journal of Computa-*  
958 *tional Physics*, 6(2), 247 – 267, doi:https://doi.org/10.1016/0021-9991(70)90024-0.
- 959 Lerche, I. (1968), Quasilinear theory of resonant diffusion in a magnetoactive, relativistic  
960 plasma, *The Physics of Fluids*, 11(8), 1720–1727, doi:10.1063/1.1692186.
- 961 Lyons, L. R. (1974), General relations for resonant particle diffusion in pitch angle and  
962 energy, *Journal of Plasma Physics*, 12(1), 45–54, doi:10.1017/S0022377800024910.
- 963 Meredith, N. P., R. B. Horne, R. M. Thorne, and R. R. Anderson (2009), Survey of upper  
964 band chorus and ech waves: Implications for the diffuse aurora, *Journal of Geophysical*  
965 *Research: Space Physics*, 114(A7), doi:10.1029/2009JA014230.
- 966 Meredith, N. P., R. B. Horne, T. Kersten, W. Li, J. Bortnik, A. Sicard, and K. H.  
967 Yearby (2018), Global model of plasmaspheric hiss from multiple satellite obser-  
968 vations, *Journal of Geophysical Research: Space Physics*, 123(6), 4526–4541, doi:  
969 10.1029/2018JA025226.
- 970 Meredith, N. P., R. B. Horne, M. A. Clilverd, and J. P. J. Ross (2019), An investigation of  
971 vlf transmitter wave power in the inner radiation belt and slot region, *Journal of Geo-*  
972 *physical Research: Space Physics*, 0(ja), doi:10.1029/2019JA026715.
- 973 Metzler, R., and J. Klafter (2000), The random walk's guide to anomalous dif-  
974 fusion: a fractional dynamics approach, *Physics Reports*, 339(1), 1 – 77, doi:  
975 https://doi.org/10.1016/S0370-1573(00)00070-3.
- 976 Mourenas, D., X.-J. Zhang, A. V. Artemyev, V. Angelopoulos, R. M. Thorne, J. Bortnik,  
977 A. I. Neishtadt, and A. A. Vasiliev (2018), Electron nonlinear resonant interaction with  
978 short and intense parallel chorus wave packets, *Journal of Geophysical Research: Space*  
979 *Physics*, 123(6), 4979–4999, doi:10.1029/2018JA025417.
- 980 Northrop, T. G. (1963), Adiabatic Charged-Particle Motion, *Reviews of Geophysics and*  
981 *Space Physics*, 1, 283–304, doi:10.1029/RG001i003p00283.
- 982 Němec, F., O. SantolÁnk, M. Parrot, and C. J. Rodger (2010), Relationship between med-  
983 ian intensities of electromagnetic emissions in the vlf range and lightning activity,  
984 *Journal of Geophysical Research: Space Physics*, 115(A8), doi:10.1029/2010JA015296.
- 985 Omidi, N., R. M. Thorne, and J. Bortnik (2010), Nonlinear evolution of emic waves in a  
986 uniform magnetic field: 1. hybrid simulations, *Journal of Geophysical Research: Space*  
987 *Physics*, 115(A12), doi:10.1029/2010JA015607.
- 988 Omidi, N., R. Thorne, and J. Bortnik (2011), Hybrid simulations of emic waves in a  
989 dipolar magnetic field, *Journal of Geophysical Research: Space Physics*, 116(A9), doi:  
990 10.1029/2011JA016511.
- 991 Omura, Y., Y. Katoh, and D. Summers (), Theory and simulation of the generation of  
992 whistler-mode chorus, *Journal of Geophysical Research: Space Physics*, 113(A4), doi:

- 993 10.1029/2007JA012622.
- 994 Omura, Y., N. Furuya, and D. Summers (2007), Relativistic turning acceleration of reso-  
995 nant electrons by coherent whistler mode waves in a dipole magnetic field, *Journal of*  
996 *Geophysical Research: Space Physics*, 112(A6), doi:10.1029/2006JA012243.
- 997 Omura, Y., M. Hikishima, Y. Katoh, D. Summers, and S. Yagitani (2009), Nonlinear  
998 mechanisms of lower-band and upper-band VLF chorus emissions in the magnetosphere,  
999 *JGR: Space Physics*.
- 1000 Perrone, D., R. O. Dendy, I. Furno, R. Sanchez, G. Zimbardo, A. Bovet, A. Fasoli,  
1001 K. Gustafson, S. Perri, P. Ricci, and F. Valentini (2013), Nonclassical transport and  
1002 particle-field coupling: from laboratory plasmas to the solar wind, *Space Science Re-*  
1003 *views*, 178(2), 233–270, doi:10.1007/s11214-013-9966-9.
- 1004 Ratcliffe, H., and C. E. J. Watt (2017), Self-consistent formation of a 0.5 cyclotron fre-  
1005 quency gap in magnetospheric whistler mode waves, *Journal of Geophysical Research:*  
1006 *Space Physics*, 122(8), 8166–8180, doi:10.1002/2017JA024399, 2017JA024399.
- 1007 Reeves, G. D., H. E. Spence, M. G. Henderson, S. K. Morley, R. H. W. Friedel, H. O.  
1008 Funsten, D. N. Baker, S. G. Kanekal, J. B. Blake, J. F. Fennell, S. G. Claudepierre,  
1009 R. M. Thorne, D. L. Turner, C. A. Kletzing, W. S. Kurth, B. A. Larsen, and J. T.  
1010 Niehof (2013), Electron Acceleration in the Heart of the Van Allen Radiation Belts,  
1011 *Science*, 341(6149), 991–994.
- 1012 Roederer, J., and H. Zhang (2013), *Dynamics of Magnetically Trapped Particles: Foun-*  
1013 *ditions of the Physics of Radiation Belts and Space Plasmas*, Astrophysics and Space  
1014 Science Library, Springer Berlin Heidelberg.
- 1015 Roederer, J. G., and S. Lejosne (2018), Coordinates for representing radiation belt par-  
1016 ticle flux, *Journal of Geophysical Research: Space Physics*, 123(2), 1381–1387, doi:  
1017 10.1002/2017JA025053.
- 1018 Schulz, M., and L. Lanzerotti (1974), *Particle diffusion in the radiation belts*, Physics and  
1019 chemistry in space, Springer-Verlag.
- 1020 Silva, C. L., S. Wu, R. E. Denton, M. K. Hudson, and R. M. Millan (2017), Hybrid fluid-  
1021 particle simulation of whistler-mode waves in a compressed dipole magnetic field: Im-  
1022 plications for dayside high-latitude chorus, *Journal of Geophysical Research: Space*  
1023 *Physics*, 122(1), 432–448, doi:10.1002/2016JA023446.
- 1024 Silva, C. L., R. E. Denton, M. K. Hudson, R. M. Millan, K. Liu, and J. Bortnik (2018),  
1025 Test-particle simulations of linear and nonlinear interactions between a 2-d whistler-  
1026 mode wave packet and radiation belt electrons, *Geophysical Research Letters*, 45(11),  
1027 5234–5245, doi:10.1029/2018GL077877.
- 1028 Stix, T. (1992), *Waves in Plasmas*, American Inst. of Physics.
- 1029 Summers, D. (2005), Quasi-linear diffusion coefficients for field-aligned electromagnetic  
1030 waves with applications to the magnetosphere, *Journal of Geophysical Research: Space*  
1031 *Physics*, 110(A8), doi:10.1029/2005JA011159.
- 1032 Sydora, R. (1999), Low-noise electromagnetic and relativistic particle-in-cell plasma sim-  
1033 ulation models, *Journal of Computational and Applied Mathematics*, 109(1), 243 – 259,  
1034 doi:https://doi.org/10.1016/S0377-0427(99)00161-2.
- 1035 Tao, X., and J. Bortnik (2010), Nonlinear interactions between relativistic radiation belt  
1036 electrons and oblique whistler mode waves, *Nonlinear Processes in Geophysics*, 17(5),  
1037 599–604, doi:10.5194/npg-17-599-2010.
- 1038 Tao, X., J. Bortnik, J. M. Albert, K. Liu, and R. M. Thorne (2011), Comparison of quasi-  
1039 linear diffusion coefficients for parallel propagating whistler mode waves with test parti-  
1040 cle simulations, *Geophysical Research Letters*, 38(6), doi:10.1029/2011GL046787.
- 1041 Tao, X., J. Bortnik, R. M. Thorne, J. M. Albert, and W. Li (2012a), Effects of amplitude  
1042 modulation on nonlinear interactions between electrons and chorus waves, *Geophysical*  
1043 *Research Letters*, 39(6), n/a–n/a, doi:10.1029/2012GL051202.
- 1044 Tao, X., J. Bortnik, R. M. Thorne, J. M. Albert, and W. Li (2012b), Effects of amplitude  
1045 modulation on nonlinear interactions between electrons and chorus waves, *Geophysical*  
1046 *Research Letters*, 39(6), doi:10.1029/2012GL051202.

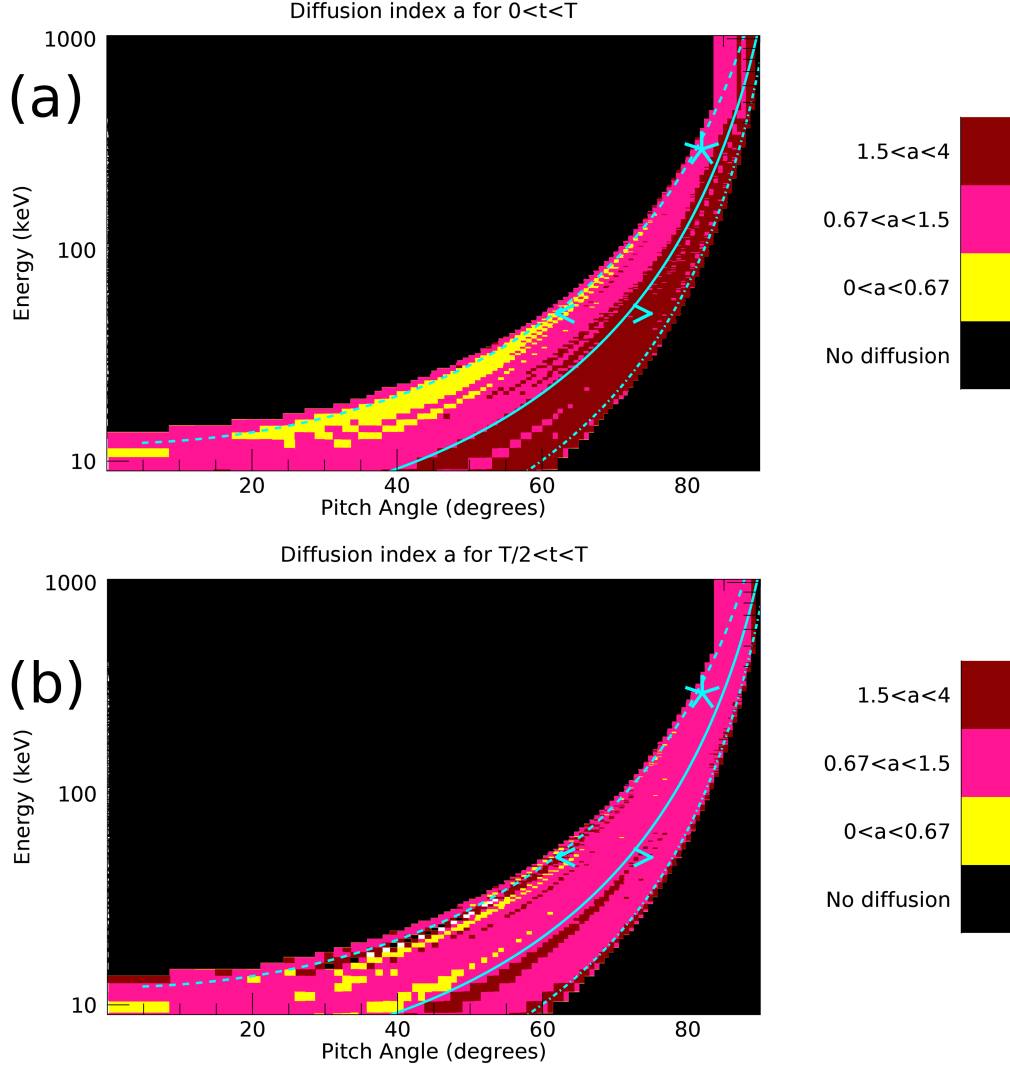
- 1047 Tao, X., J. Bortnik, J. Albert, R. Thorne, and W. Li (2013), The importance of am-  
 1048 plitude modulation in nonlinear interactions between electrons and large amplitude  
 1049 whistler waves, *Journal of Atmospheric and Solar-Terrestrial Physics*, *99*, 67 – 72, doi:  
 1050 <https://doi.org/10.1016/j.jastp.2012.05.012>, dynamics of the Complex Geospace System.
- 1051 Thorne, R. M. (2010), Radiation belt dynamics: The importance of wave-particle interac-  
 1052 tions, *Geophysical Research Letters*, *37*(22), doi:10.1029/2010GL044990.
- 1053 Thorne, R. M., B. Ni, X. Tao, R. B. Horne, and N. P. Meredith (2010), Scattering by cho-  
 1054 rus waves as the dominant cause of diffuse auroral precipitation, *Nature*, *467*, 943–946,  
 1055 doi:10.1038/nature09467.
- 1056 Thorne, R. M., W. Li, B. Ni, Q. Ma, J. Bortnik, L. Chen, D. N. Baker, H. E. Spence,  
 1057 G. D. Reeves, M. G. Henderson, C. A. Kletzing, W. S. Kurth, G. B. Hospodarsky, J. B.  
 1058 Blake, J. F. Fennell, S. G. Claudepierre, and S. G. Kanekal (2013), Rapid local accel-  
 1059 eration of relativistic radiation-belt electrons by magnetospheric chorus, *Nature*, *504*,  
 1060 411–414, doi:10.1038/nature12889.
- 1061 Treumann, R. A., and W. Baumjohann (2001), *Advanced Space Plasma Physics*, Imperial  
 1062 College Press.
- 1063 Tsiklauri, D. (2016), The effect of a longitudinal density gradient on electron plasma wake  
 1064 field acceleration, *Proceedings of the Royal Society A: Mathematical, Physical and Engi-  
 1065 neering Sciences*, *472*(2196), 20160,630, doi:10.1098/rspa.2016.0630.
- 1066 Tsurutani, B. T., and E. J. Smith (1977), Two types of magnetospheric elf chorus and their  
 1067 substorm dependences, *Journal of Geophysical Research (1896-1977)*, *82*(32), 5112–  
 1068 5128, doi:10.1029/JA082i032p05112.
- 1069 Vainchtein, D., X.-J. Zhang, A. V. Artemyev, D. Mourenas, V. Angelopoulos, and R. M.  
 1070 Thorne (2018), Evolution of electron distribution driven by nonlinear resonances with  
 1071 intense field-aligned chorus waves, *Journal of Geophysical Research: Space Physics*,  
 1072 *0*(0), doi:10.1029/2018JA025654.
- 1073 Villaseñor, J., and O. Buneman (1992), Rigorous charge conservation for local elec-  
 1074 tromagnetic field solvers, *Computer Physics Communications*, *69*(2), 306 – 316, doi:  
 1075 [https://doi.org/10.1016/0010-4655\(92\)90169-Y](https://doi.org/10.1016/0010-4655(92)90169-Y).
- 1076 Wilson III, L. B., C. A. Cattell, P. J. Kellogg, J. R. Wygant, K. Goetz, A. Breneman, and  
 1077 K. Kersten (2011), The properties of large amplitude whistler mode waves in the mag-  
 1078 netosphere: Propagation and relationship with geomagnetic activity, *Geophys. Res. Lett.*,  
 1079 *38*, doi:10.1029/2011GL048671.
- 1080 Zaslavsky, G. (2002), Chaos, fractional kinetics, and anomalous transport, *Physics Reports*,  
 1081 *371*(6), 461 – 580, doi:[https://doi.org/10.1016/S0370-1573\(02\)00331-9](https://doi.org/10.1016/S0370-1573(02)00331-9).
- 1082 Zhang, X.-J., R. Thorne, A. Artemyev, D. Mourenas, V. Angelopoulos, J. Bortnik, C. A.  
 1083 Kletzing, W. S. Kurth, and G. B. Hospodarsky (2018a), Properties of intense field-  
 1084 aligned lower-band chorus waves: Implications for nonlinear wave-particle inter-  
 1085 actions, *Journal of Geophysical Research: Space Physics*, *123*(7), 5379–5393, doi:  
 1086 10.1029/2018JA025390.
- 1087 Zhang, Z., L. Chen, X. Li, Z. Xia, R. A. Heelis, and R. B. Horne (2018b), Observed  
 1088 propagation route of vlf transmitter signals in the magnetosphere, *Journal of Geophys-  
 1089 ical Research: Space Physics*, *123*(7), 5528–5537, doi:10.1029/2018JA025637.
- 1090 Zimbardo, G., E. Amato, A. Bovet, F. Effenberger, A. Fasoli, H. Fichtner, I. Furno,  
 1091 K. Gustafson, P. Ricci, S. Perri, and et al. (2015), Superdiffusive transport in labo-  
 1092 ratory and astrophysical plasmas, *Journal of Plasma Physics*, *81*(6), 495810,601, doi:  
 1093 10.1017/S0022377815001117.



556 **Figure 7.**  $\text{var}(\alpha_i)$  for three bins roughly centred on: (a): $(E, \alpha) = (20\text{keV}, 45^\circ)$ , (b): $(E, \alpha) = (300\text{keV}, 82^\circ)$ ,  
 557 and (c): $(50\text{keV}, 75^\circ)$  respectively. Asterisks mark the particle data, and solid black lines mark curve fits. The  
 558 solid blue line is a linear fit over  $T/2 < \tilde{t} < T$ .



597 **Figure 8.**  $\text{var}(\alpha_I)$  for a bin roughly centred on  $(E, \alpha) = (9.2\text{keV}, 40^\circ)$ . Asterisks mark the particle data,  
 598 solid black lines is a curve fits, and the solid blue line is a linear fit over  $T/2 < \tilde{t} < T$ . The solid green line  
 599 shows evolution of  $\text{var}(\alpha)$  consistent with the PADIE diffusion coefficient,  $D_{\alpha\alpha}$ , over  $T/2 < \tilde{t} < T$ .



638 **Figure 9.** The diffusion index,  $a$ , for each  $(E, \alpha)$  bin in the experiment. Plot(a) shows this index over the  
 639 entire time of wave-particle interaction ( $0 < \tilde{t} < T$ ), whereas plot (b) shows the index for the second half  
 640 of the interaction only ( $T/2 < \tilde{t} < T$ ). Black indicates ‘no diffusion’. Yellow indicates ‘sub-diffusion’  
 641 ( $0 < a < 0.67$ ), pink indicates normal diffusion ( $0.67 < a < 1.5$ ), and dark red regions indicate super-  
 642 diffusion ( $a > 1.5$ ). The over-plotted cyan curves mark the values of energy and pitch angle that are (accord-  
 643 ing to equations (4) and (5)) in “ $n = -1$  resonance” with waves of frequency  $f_{lc}$  (‘dash’),  $f_{uc}$  (‘dash-dot’),  
 644 and  $0.5(f_{lc} + f_{uc})$  (‘solid’). The bins represented in figure 7(a)-(c) are marked by cyan symbols: “ $<$ ”, “ $\star$ ” and  
 645 “ $>$ ”.

Figure 1.

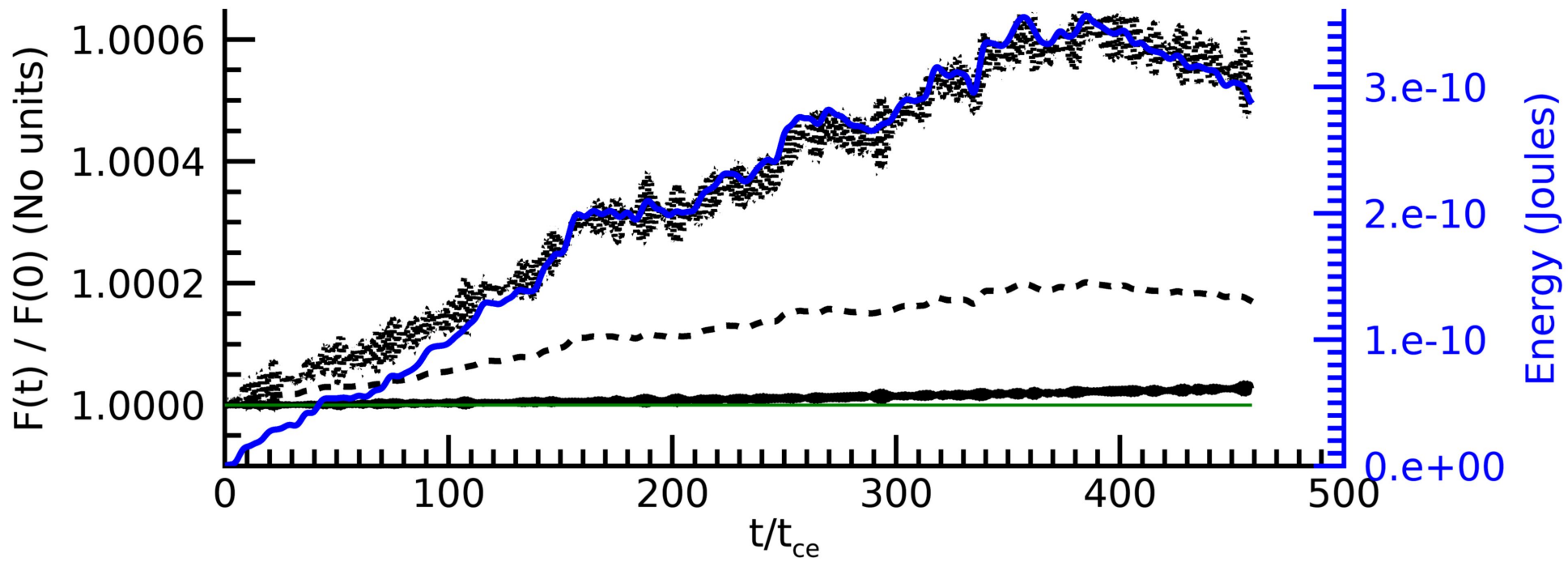
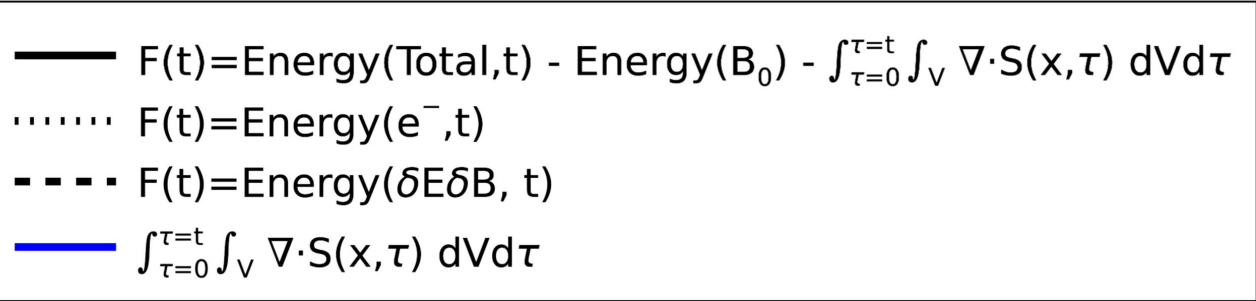




Figure 2.

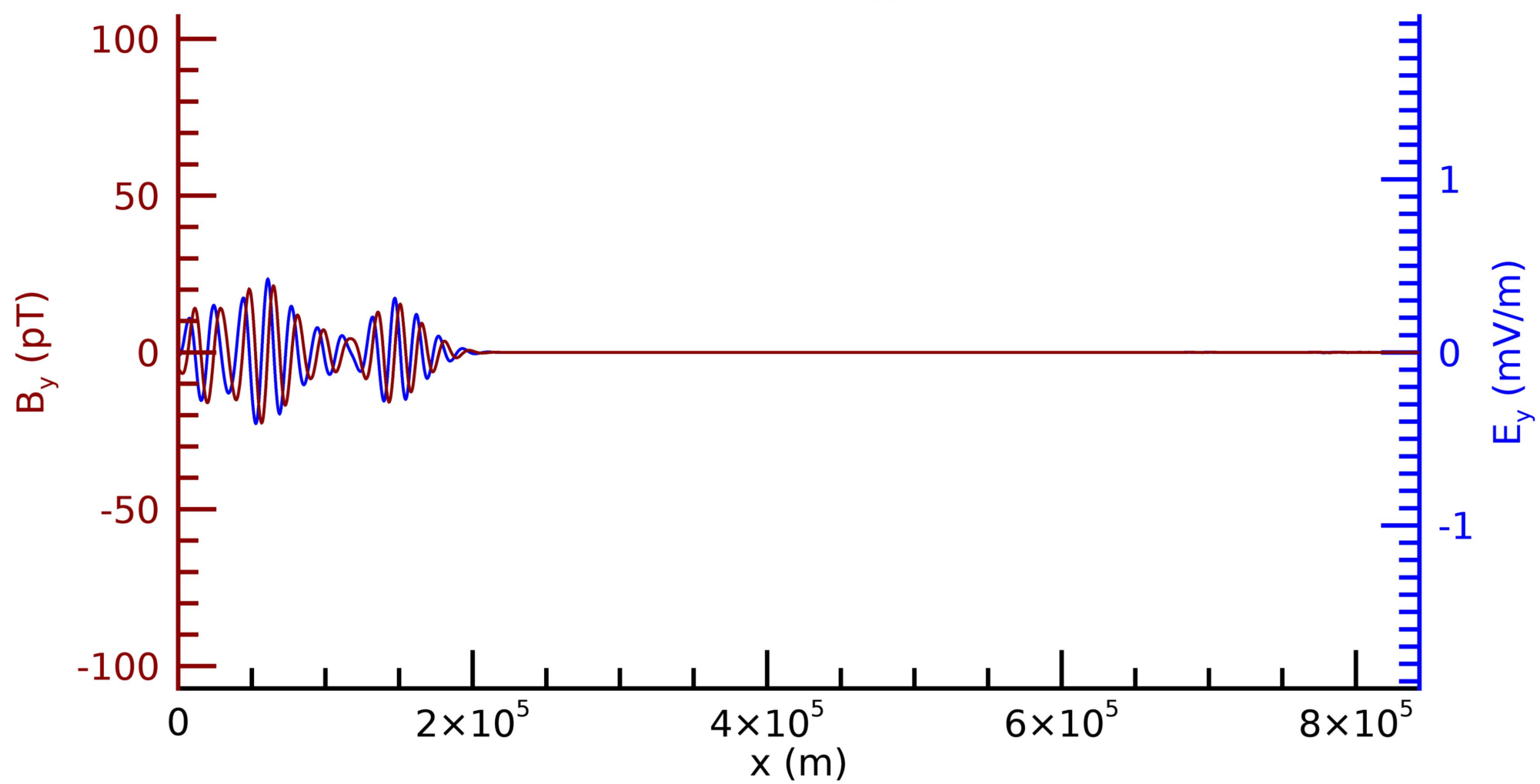
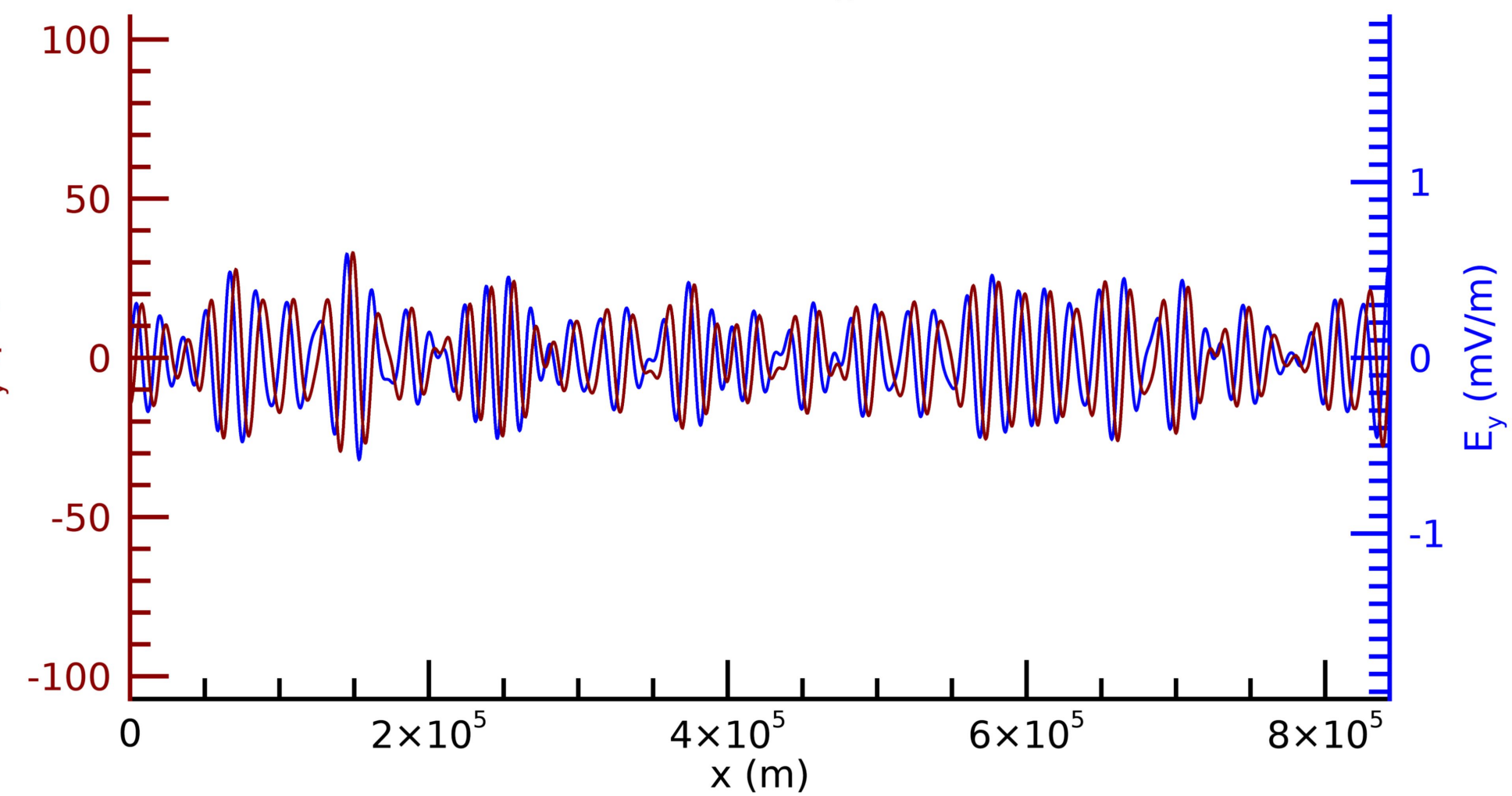
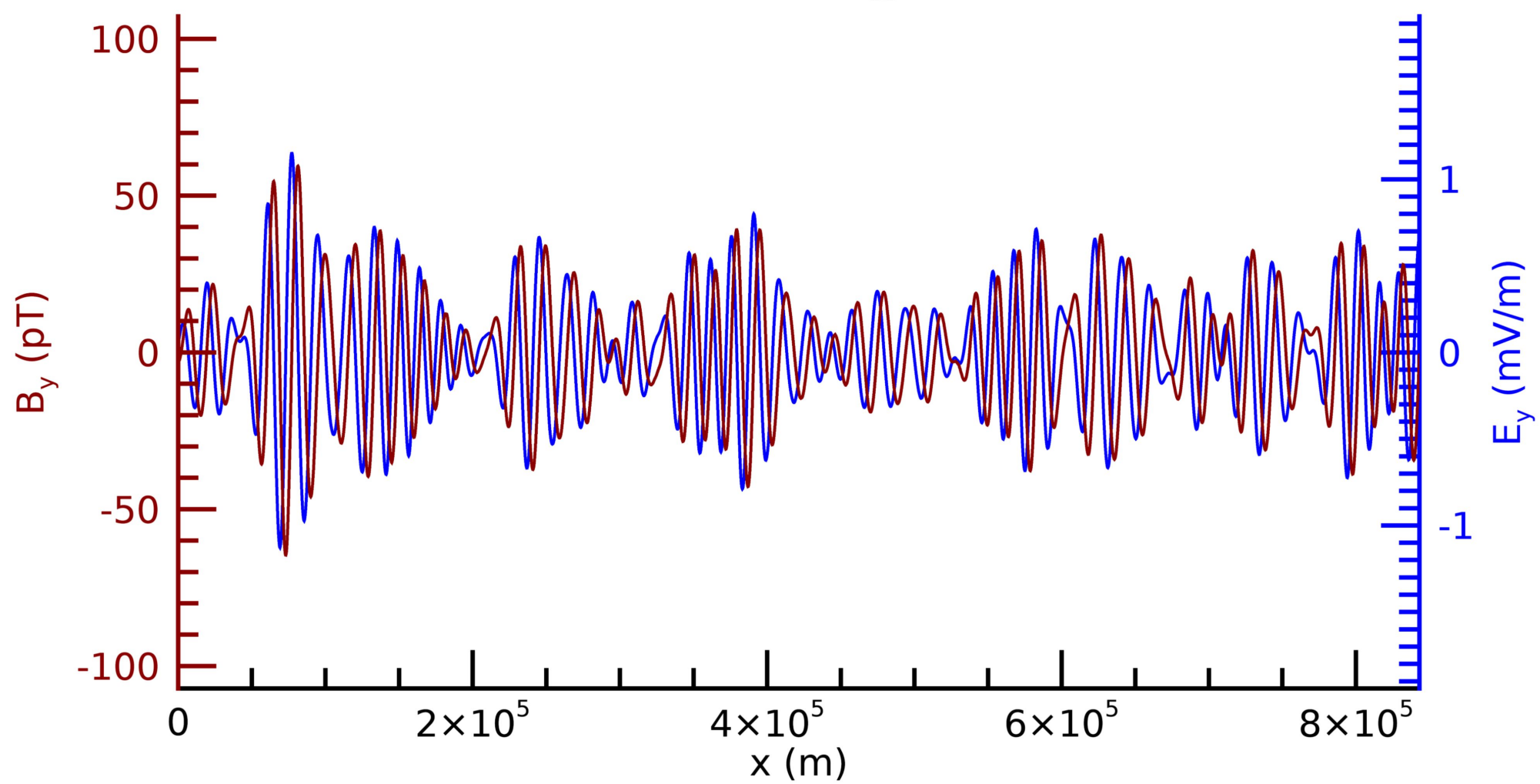
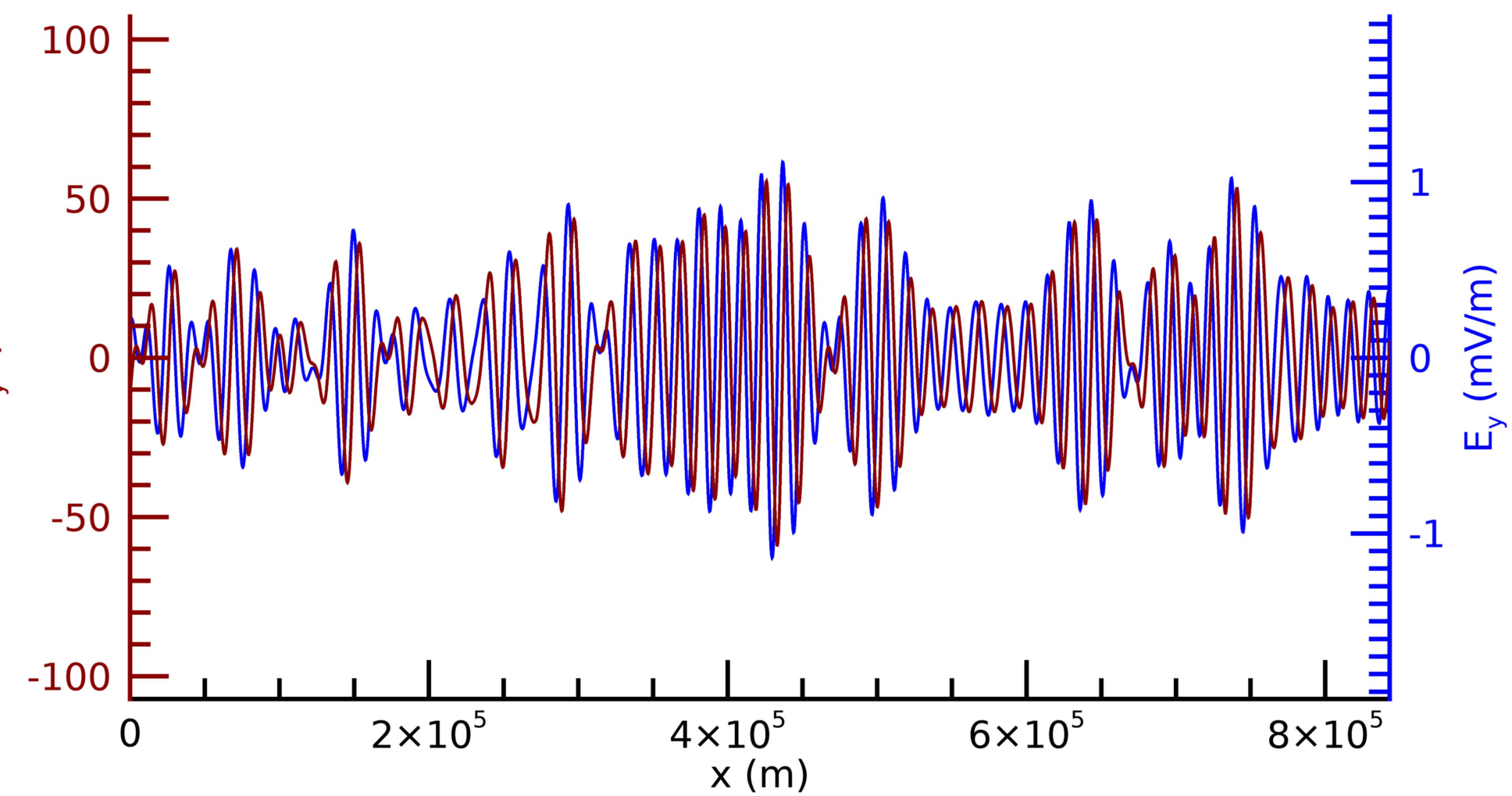
**(a)** $t = 028 t_{ce}$ **(b)** $t = 143 t_{ce}$ **(c)** $t = 280 t_{ce}$ **(d)** $t = 561 t_{ce}$ 

Figure 3.

Fourier Amplitude of  $E_y$  and  $B_y$  components

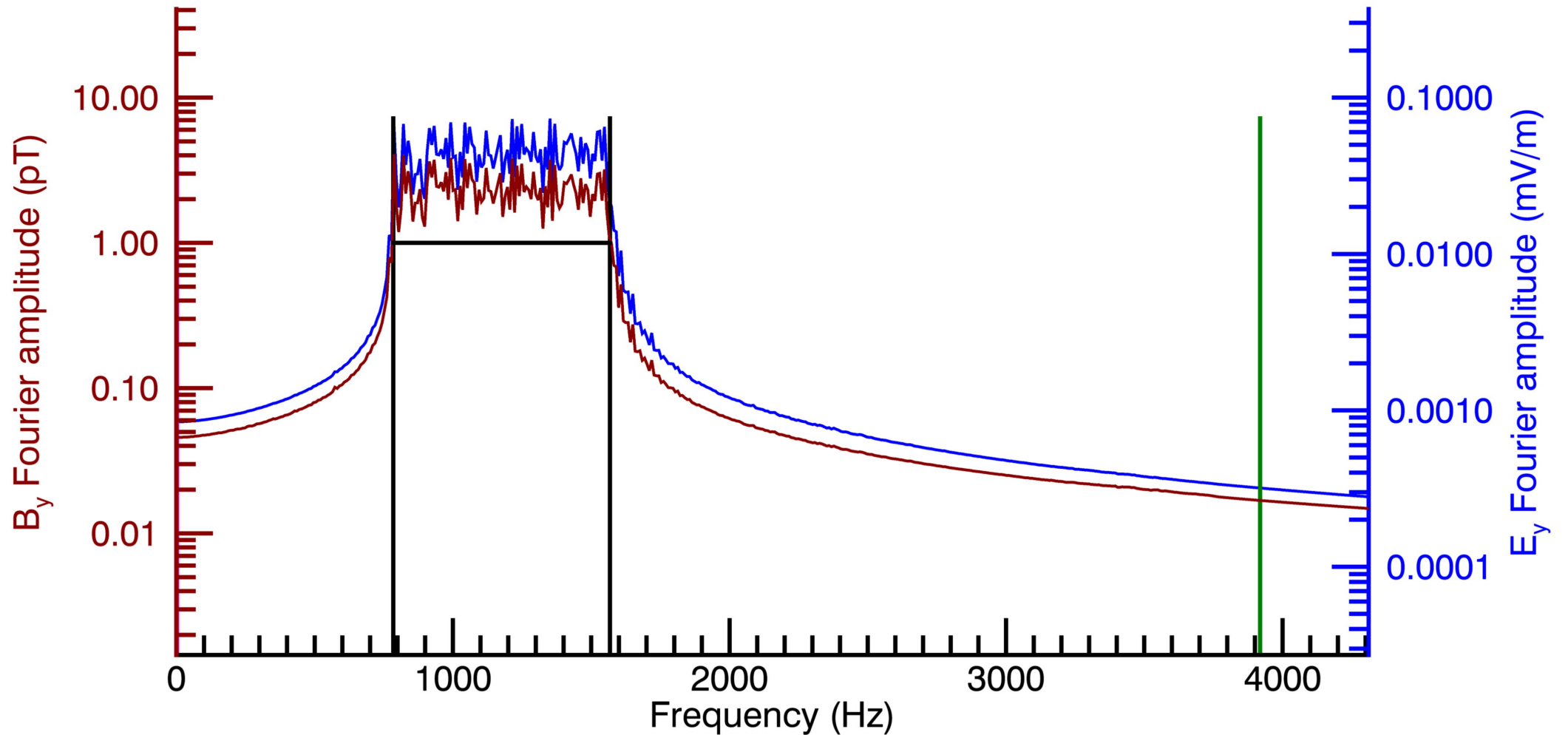


Figure 4.

# Dispersion relation for $B_y$

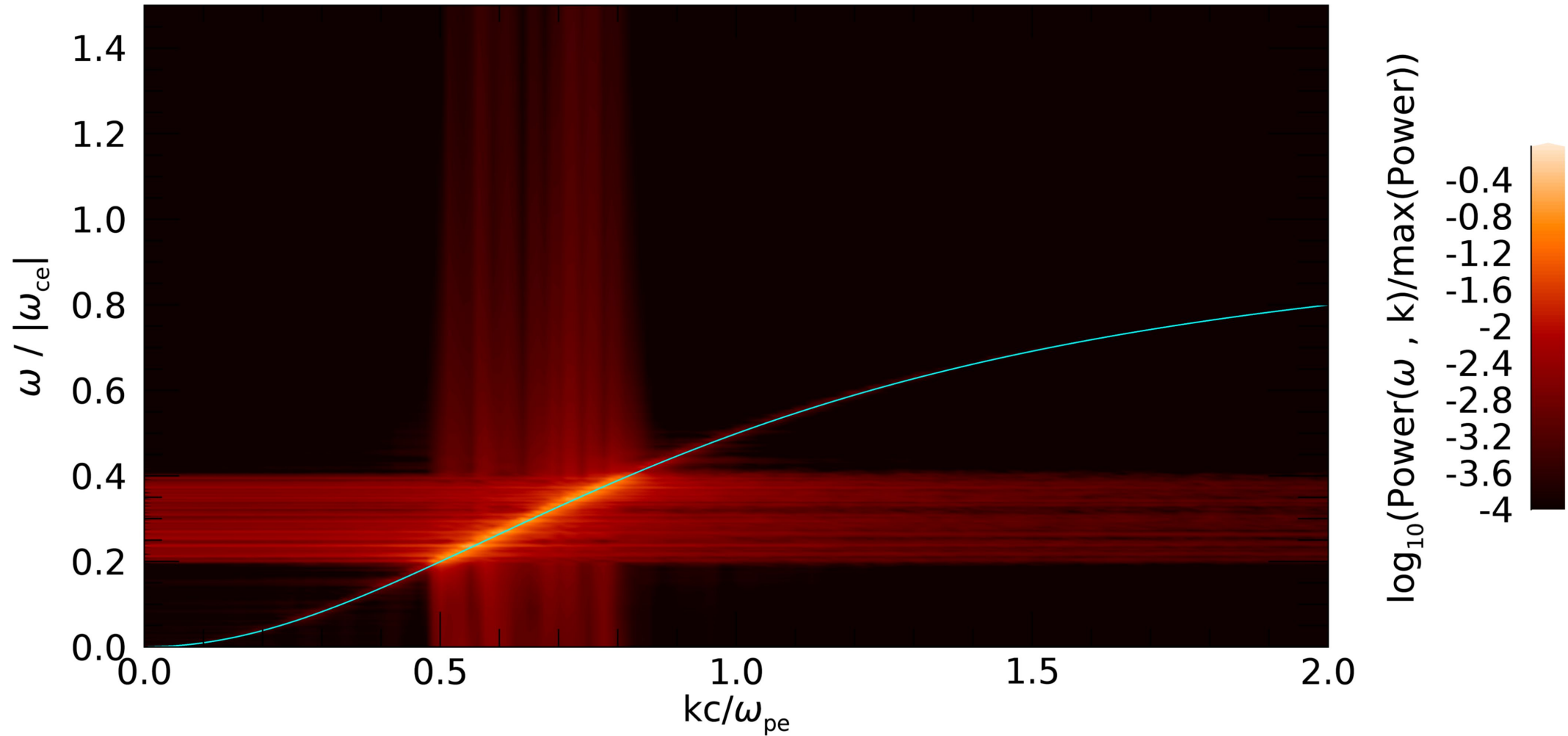


Figure 5.

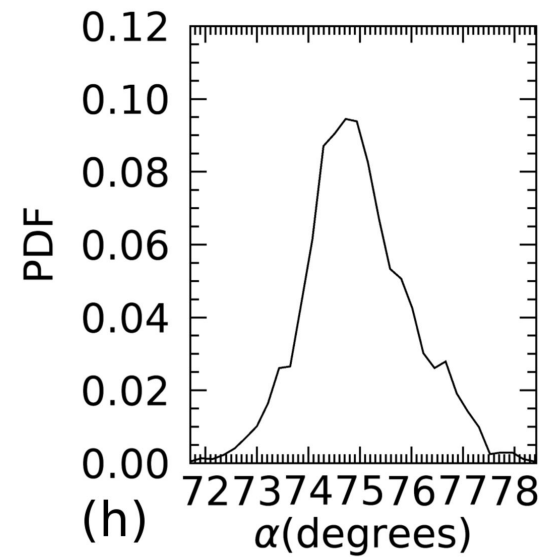
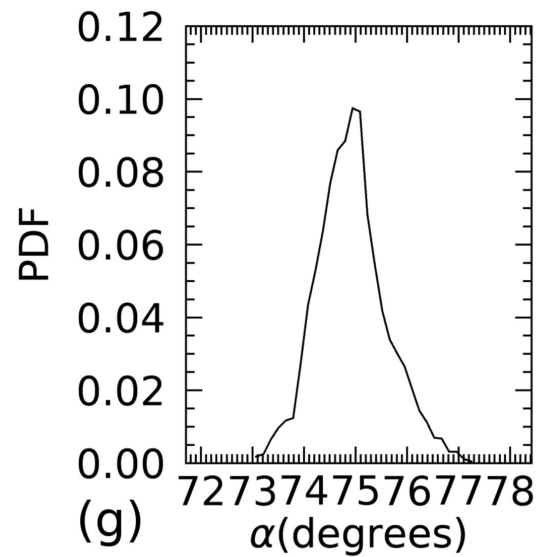
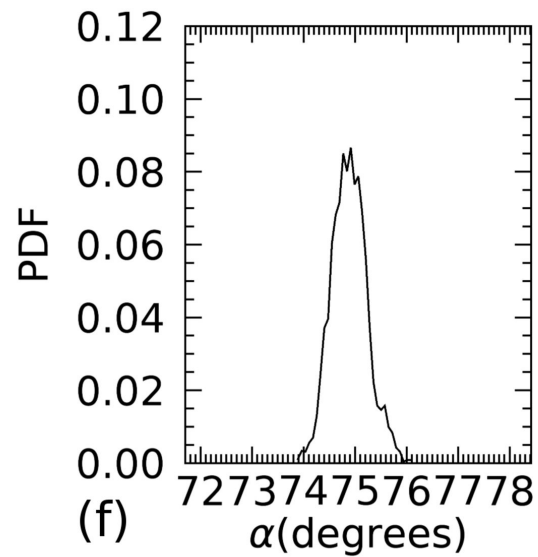
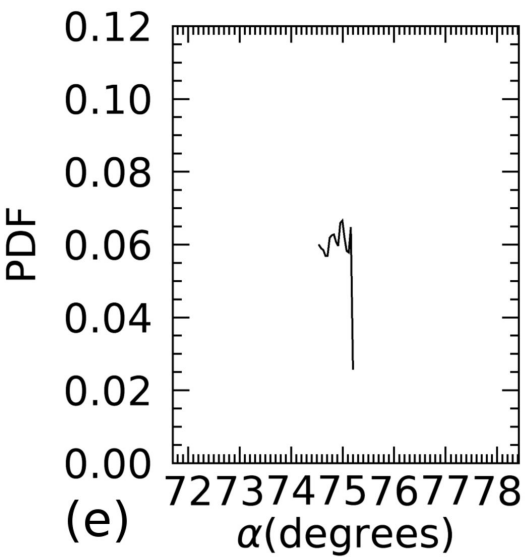
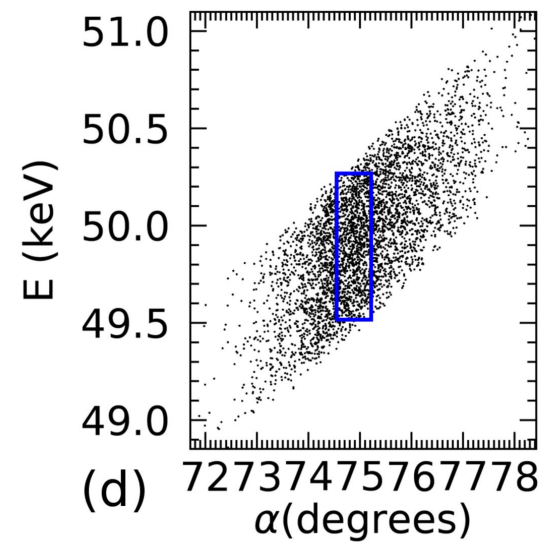
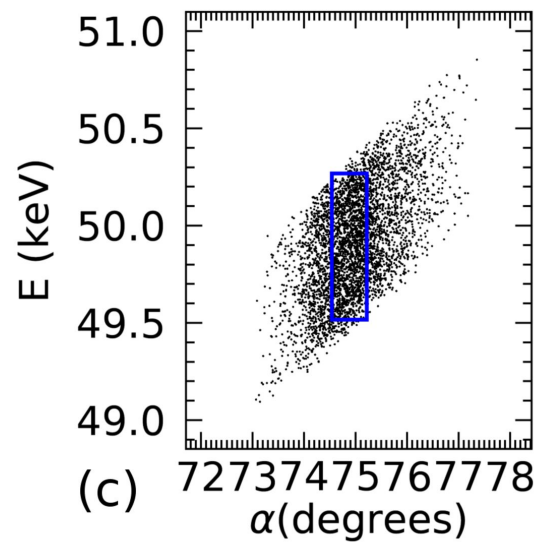
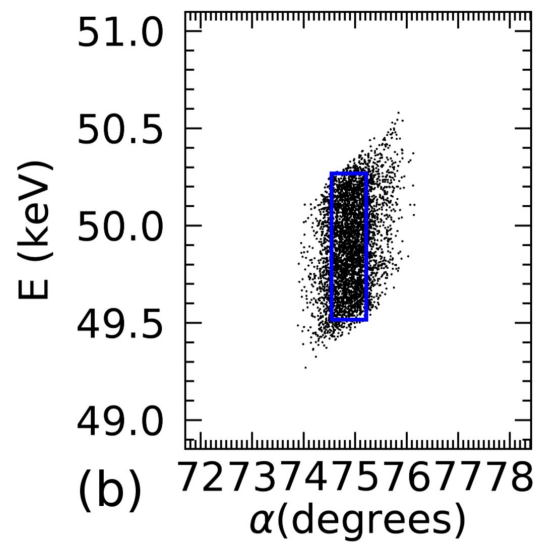
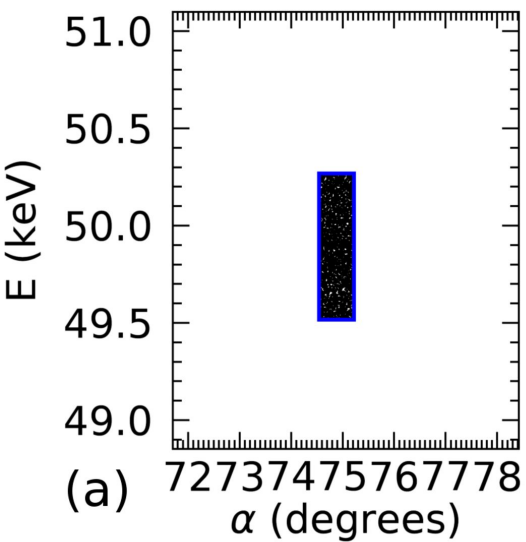




Figure 6.

$d\alpha(E, \alpha)$

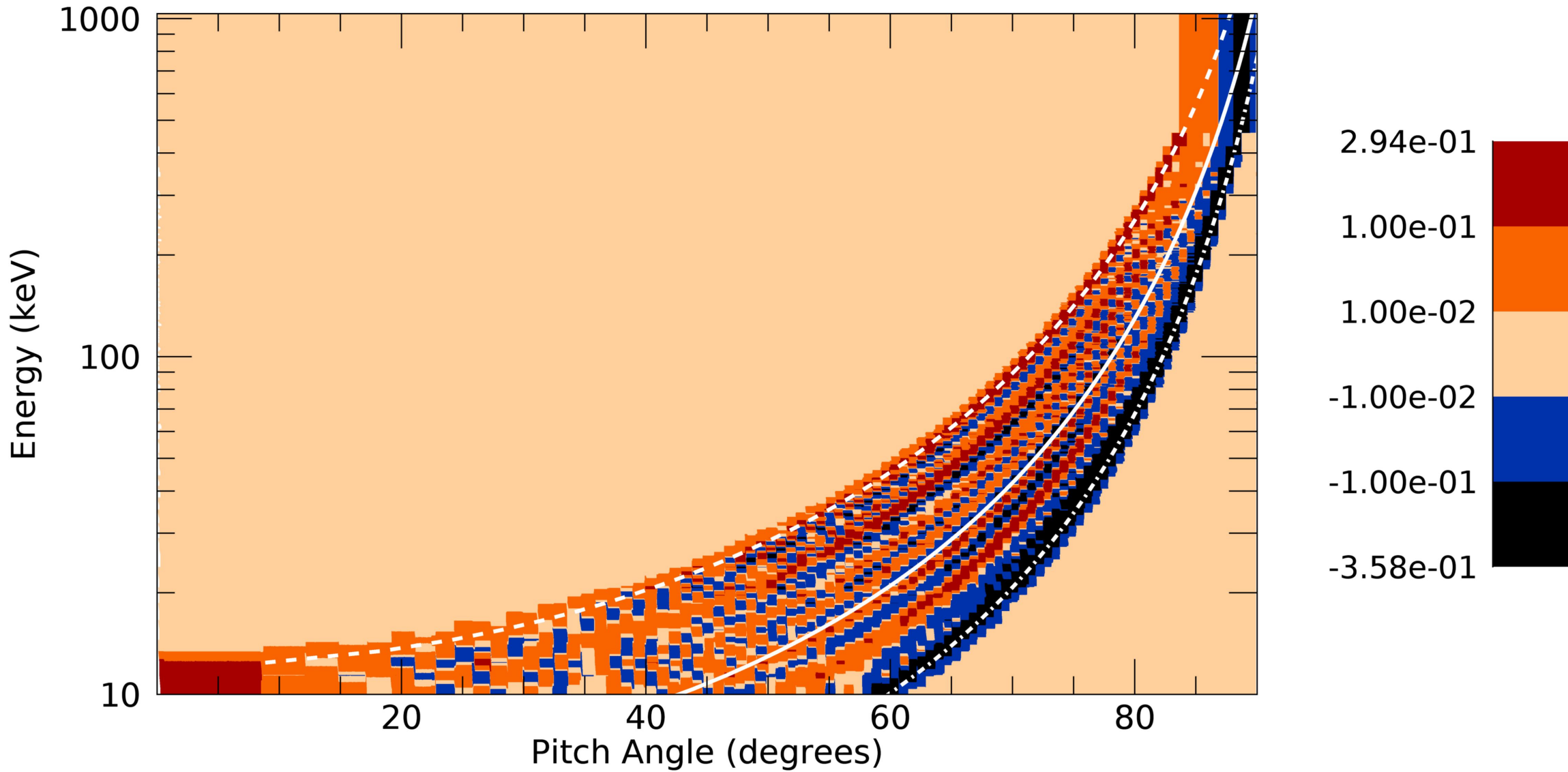


Figure 7.

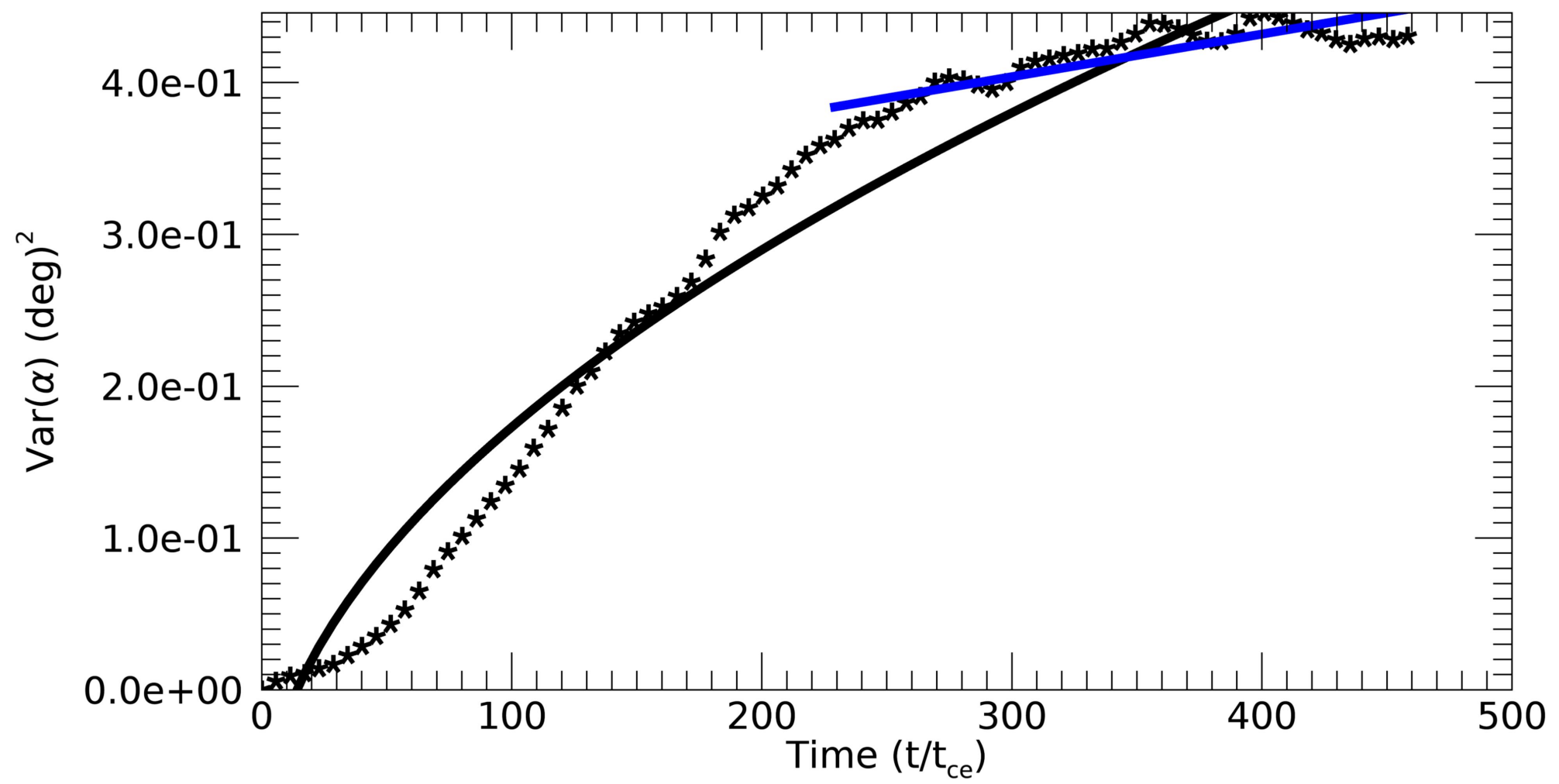
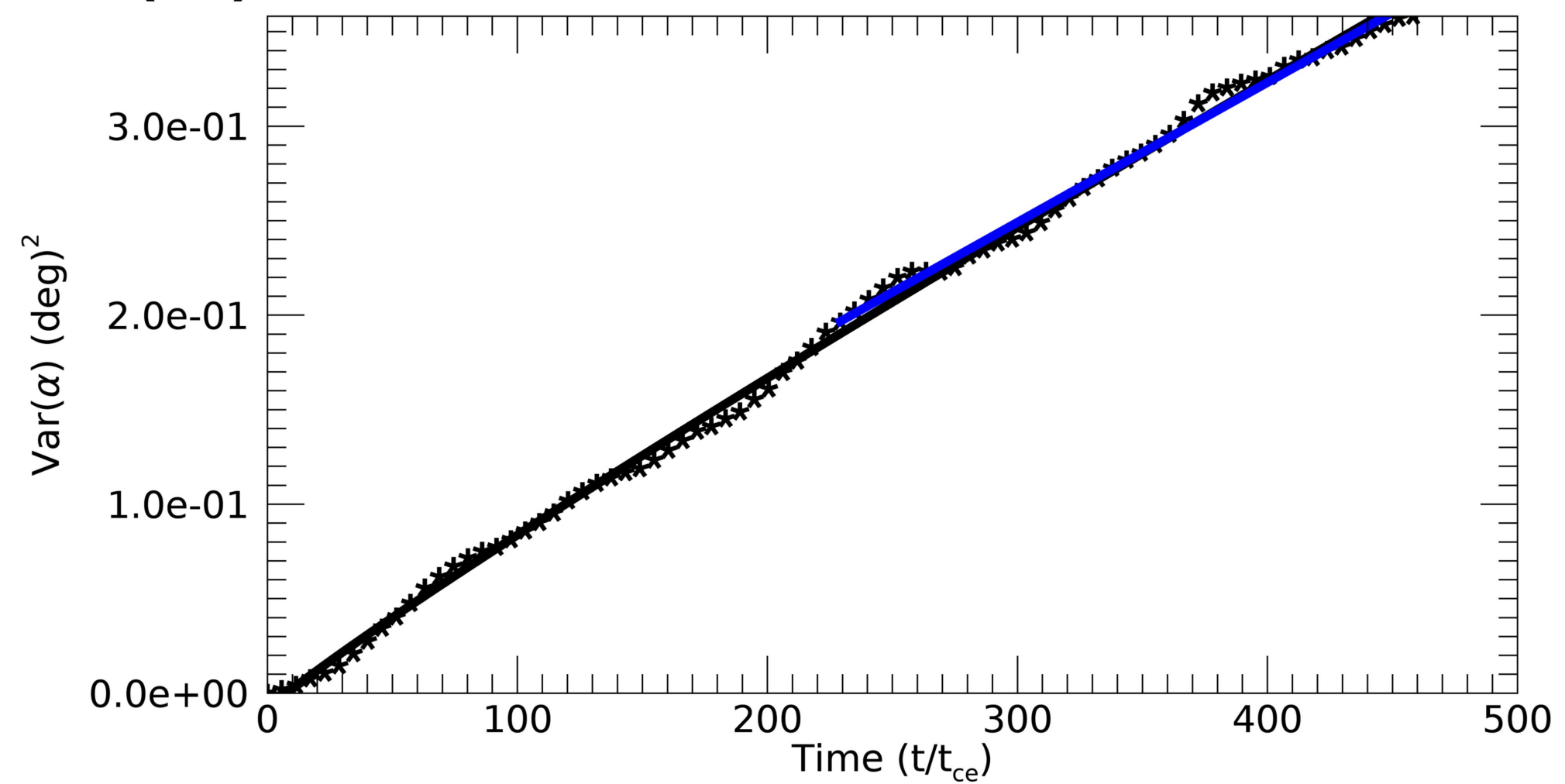
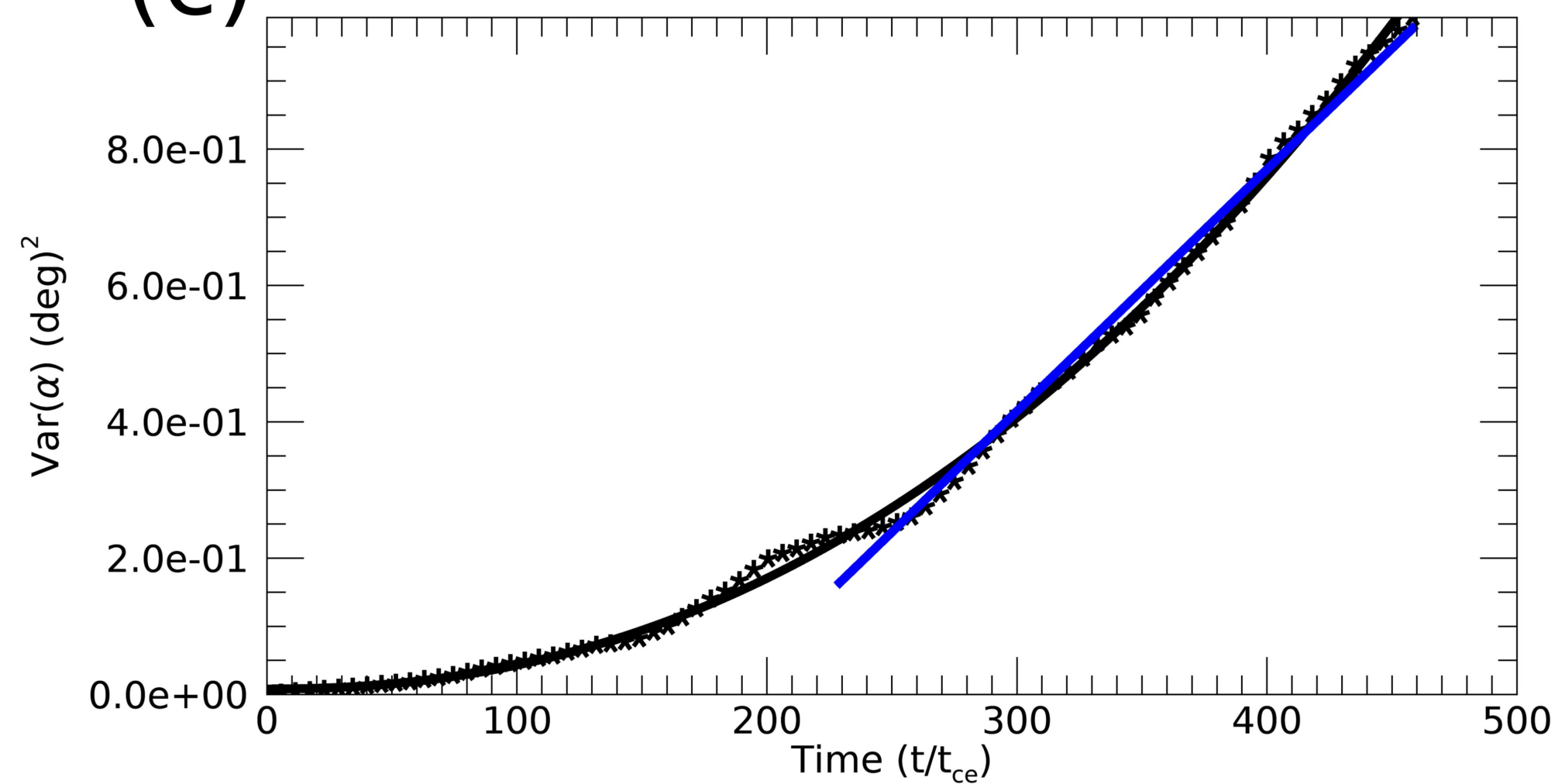
**(a)**Var( $\alpha$ ) for E=20.00 keV,  $\alpha=45.00$ , "a"=0.516**(b)**Var( $\alpha$ ) for E=300.00 keV,  $\alpha=82.00$ , "a"=0.924**(c)**Var( $\alpha$ ) for E=50.00 keV,  $\alpha=75.00$ , "a"=2.21

Figure 8.

Var( $\alpha$ ) for E=9.22 keV,  $\alpha=40.00$ , "a"=1.15

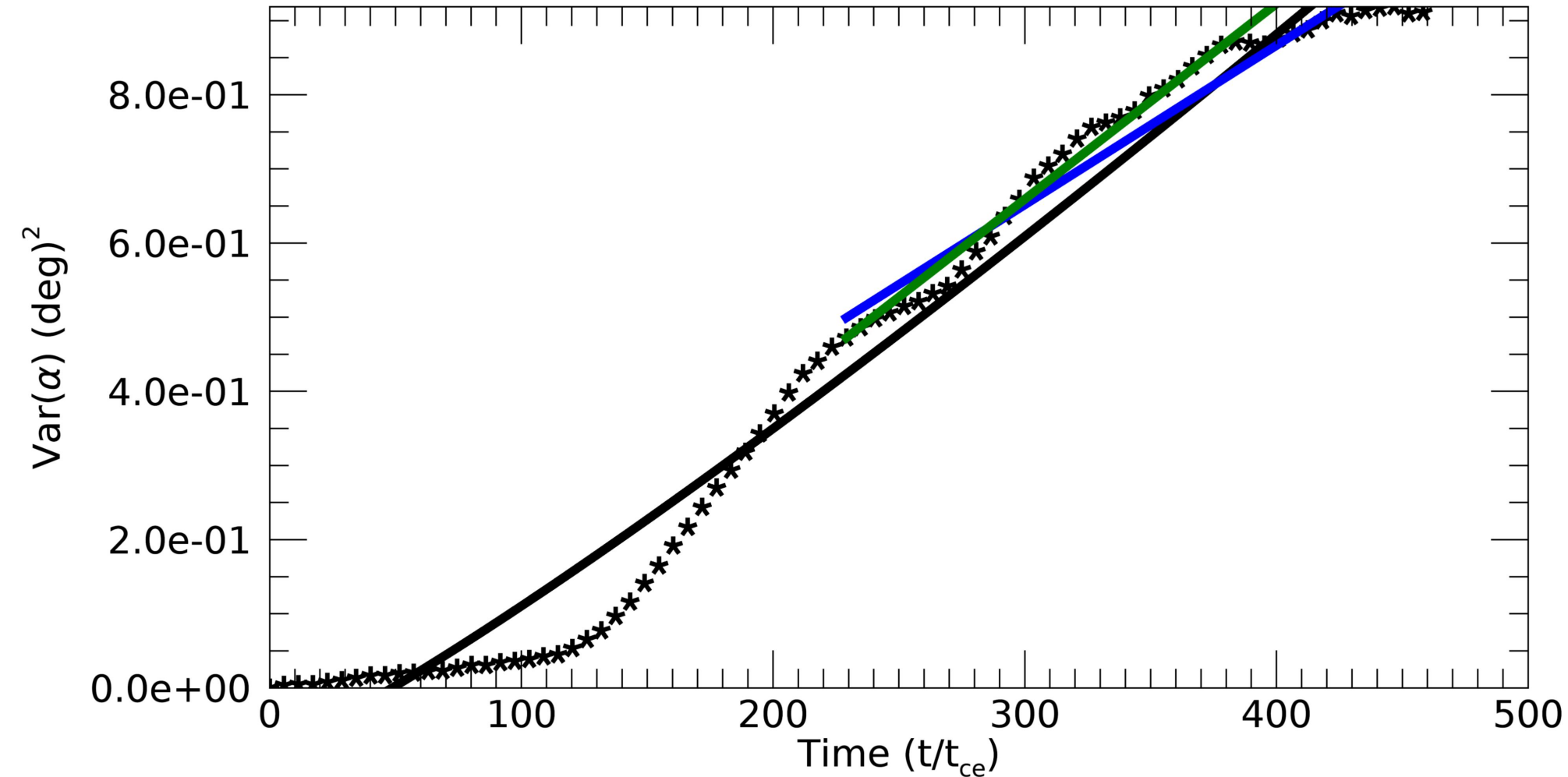
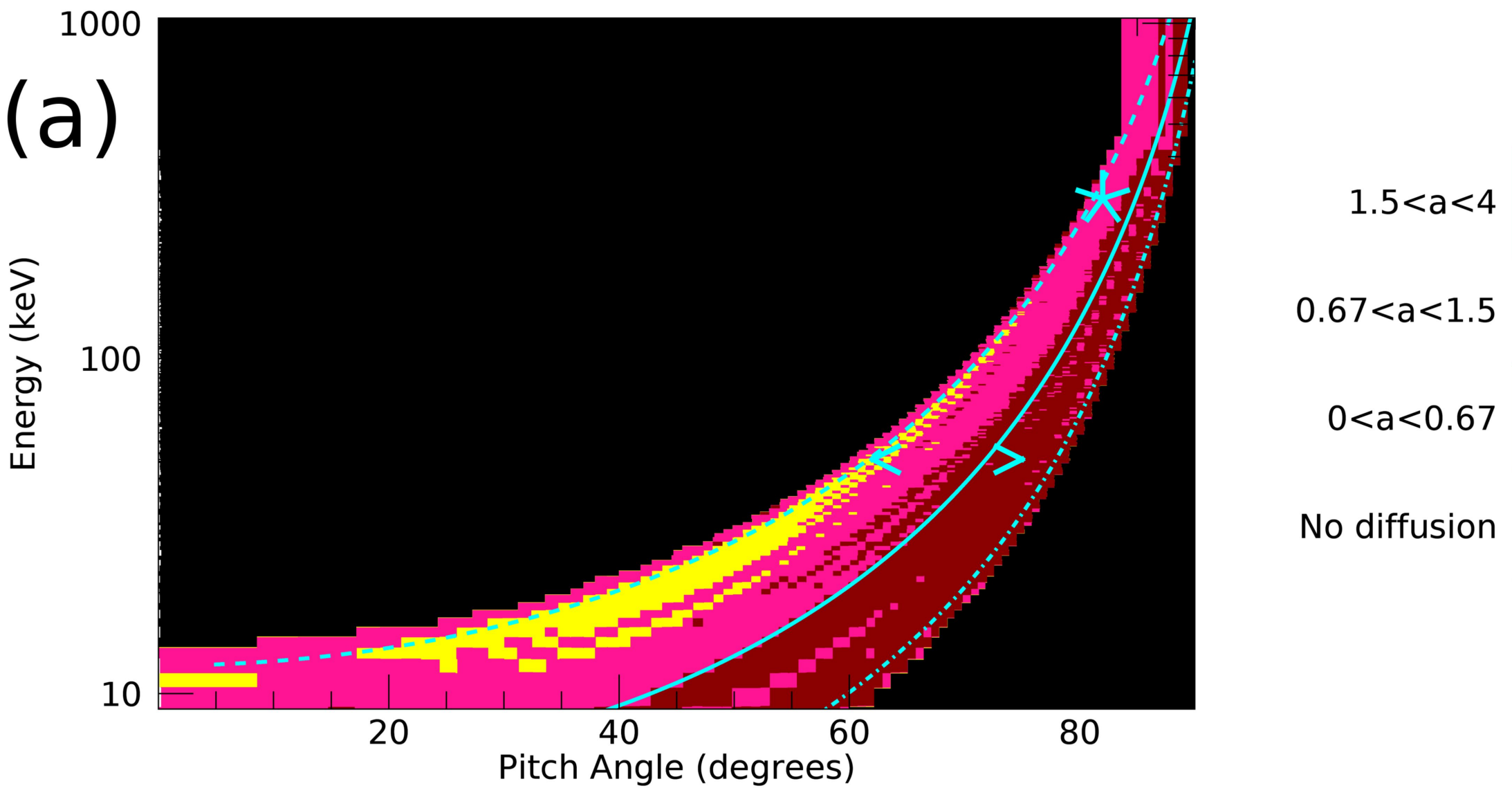


Figure 9.

Diffusion index a for  $0 < t < T$



Diffusion index a for  $T/2 < t < T$

